Inversion of earthquake focal mechanisms to obtain the seismotectonic stress IV- a new method free of choice among nodal planes

J. Angelier

Geophys. J. Int. (2002) **150,** 588–609

Inversion of earthquake focal mechanisms to obtain the seismotectonic stress IV—a new method free of choice among nodal planes

Jacques Angelier

Séismotectonique et Tectonophysique, URA 7072, *Université Pierre et Marie Curie, Case 129, T26-E1, 4 place Jussieu,* 75252 *Paris Cedex* 05, *France.*
E-mail: jacques.angelier@lgs.jussieu.fr

Accepted 2002 February 25. Received 2002 February 1; in original form 2001 May 22

SUMMARY

A new method is presented, to obtain the stress state that best accounts for a set of double couple focal mechanisms of earthquakes. This method is based on the slip shear stress component (SSSC) criterion. The sum of the SSSC values is maximized as a function of four unknowns that describe the reduced stress tensor, including the orientations of the principal stress axes and the ratio between the principal stress differences. This new method combines two advantages. First, no choice between the nodal planes of each focal mechanism is needed, because of the intrinsic properties of the SSSC. Secondly, the runtime is negligible regardless of the size of the data set, because the inverse problem is solved by analytical means so that the numerical aspects are reduced to a minimum. For these reasons, the SSSC-based inversion is easily included in a variety of processes for separating or refining the data. A typical set of focal mechanisms of earthquakes in Taiwan is processed to illustrate the application and potential of the new method.

Key words: earthquake, focal mechanism, inversion, seismotectonics, stress, tensor.

1 THE PROBLEM

The determination of the seismotectonic regime based on the inversion of sets of focal mechanisms of earthquakes has been studied by several authors (e.g. Angelier 1984; Gephart & Fortsyth 1984; Mercier & Carey-Gailhardis 1989). Among the most prominent difficulties of such an inverse analysis were some non-linear or discontinuous mathematical aspects of the inverse problem, and an intrinsic property of the double couple focal mechanisms, which apparently required a preliminary choice between the nodal planes.

In this paper, we aim to show first that to perform the inversion of a data set and obtain the best-fitting stress tensor it is not necessary to choose between the nodal planes of the double couple focal mechanisms. Secondly, it is demonstrated that the analysis can be carried out by purely analytical means, which results in an almost instantaneous resolution of the problem regardless of the size of the data set. These two main objectives are attained through the use of a new criterion, the slip shear stress component (SSSC). Both the properties of this criterion and the mathematical and physical principles of the analytical inversion are explored. The corresponding method was mentioned in an abstract (Angelier 1998), but never described.

The inverse analysis is considered from both the mathematical and the mechanical points of view. The final aim of this paper is to illustrate the numerical application of this new method, based on consideration of a typical data set of focal mechanisms of earthquakes.

2 DEFINITION OF THE SLIP SHEAR STRESS COMPONENT

The shear stress slip component, or SSSC, is the component of stress acting in the slip direction on a fault (Fig. 1). As a vector, the SSSC, $\boldsymbol{\tau}_s$, is the orthogonal projection of the shear stress, $\boldsymbol{\tau}$, onto the slip vector, **s**. It is also the orthogonal projection on **s** of the applied stress vector, $\boldsymbol{\sigma}$. As a value, the SSSC, τ_s, is the scalar product of $\boldsymbol{\tau}$ by the unit slip vector, **s** (so that τ_s is also the scalar product of $\boldsymbol{\sigma}$ by **s**). According to this definition, τ_s may be negative, indicating that the calculated stress acts in the opposite sense to that of the observed slip. Thus, the SSSC value is not the modulus of the SSSC vector, although their absolute values are identical. Note that throughout this paper a bold symbol, such as $\boldsymbol{\tau}$, refers to a vector or a tensor (regular ones refer to scalars or vector moduli).

As an example, let us consider a fault with a movement occurring in the imposed direction of a given vector **s**. Situations where there is an imposed slip direction may result from geometrical interactions between faulted blocks: the slip cannot occur along the direction of the shear stress, $\boldsymbol{\tau}$, as would be the case for a fault left free to move in any direction in the rock mass. This example shows that the component of stress that may induce motion along **s**, the real

slip direction, is $\boldsymbol{\tau}_s$, the SSSC, instead of the shear stress itself, $\boldsymbol{\tau}$. Remember that the stress and related vectors (including $\boldsymbol{\tau}$ and $\boldsymbol{\tau}_s$) are calculated, whereas the slip vector (**s**) results from the observation.

Whether or not the slip is explained by the stress depends on the SSSC value. Within this framework, an important, albeit non-exclusive, role is played by the angle between the observed slip direction and the calculated shear stress (Fig. 1). This angle, α, is simply called the slip-shear angle hereafter. For example, with a shear stress that is at a small oblique angle to the imposed slip direction, the SSSC value is positive and close to the magnitude of the shear stress (Fig. 2a); it reaches τ for zero angle. When the angle becomes close to 90°, the SSSC value is small (Fig. 2b); it becomes zero for an angle of 90°. For an obtuse angle the SSSC value is negative; it approaches the shear stress magnitude in absolute value if the angle is large (Fig. 2c), reaching $-\tau$ for an angle of 180°. Thus, as α increases, it is more and more difficult to account for the observed slip with the calculated shear stress. For large acute angles (Fig. 2b), the small calculated stress is unlikely to explain the observed slip, unless the friction coefficient is small and the normal stress is small or negative. For angles greater than 90°, this difficulty becomes an impossibility because the SSSC acts in the opposite sense with respect to the slip vector (Fig. 2c). The situations where stress accounts well for slip belong to the type shown in Fig. 2(a), i.e. with an angle α as small as possible. This kind of criterion has been adapted in different ways in the stress analyses of fault slip data sets (Carey & Brunier 1974; Angelier 1975; Etchecopar *et al.* 1981; Michael 1984).

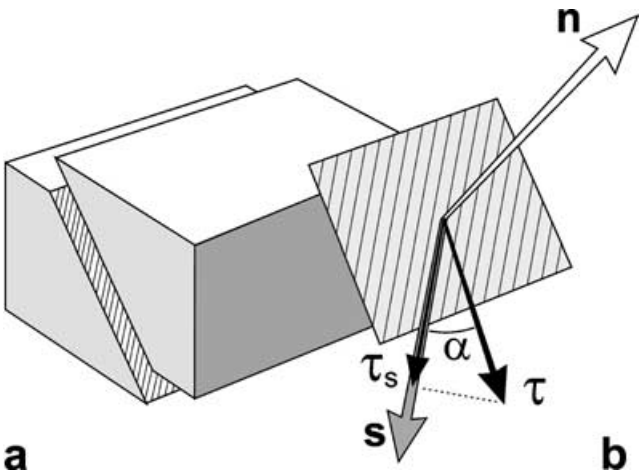

Figure 1. The shear stress slip component, or SSSC. Block diagram showing a reverse left-lateral fault. Two unit vectors define the slip: **n**, normal to fault plane, and **s,** unit slip vector. By convention, **n** (open arrow) is chosen in the upper half-space, whereas **s** (grey arrow) indicates the motion of the lower block with respect to the upper one, and hence is in the lower half-space for a reverse fault (upper half-space for a normal fault). Striations as thin lines on fault plane. Black arrows indicate the shear stress, $\boldsymbol{\tau}$, and the SSSC vector, $\boldsymbol{\tau}_s$. The angle between the calculated shear stress and the actual slip is α (slip-shear angle).

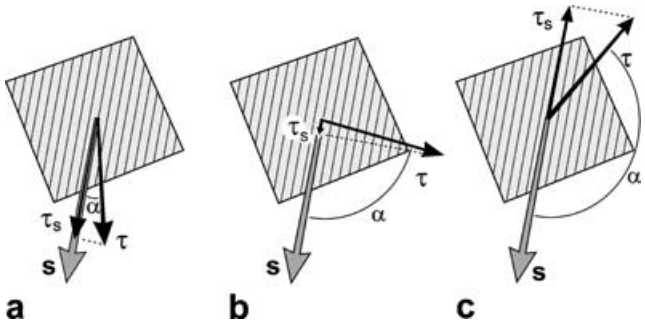

Figure 2. Variation of the SSSC value (τ_s) as a function of the slip-shear angle (α). Unit slip vector as **s** (grey arrow); shear stress, $\boldsymbol{\tau}$; and SSSC vector, $\boldsymbol{\tau}_s$ (black arrows). Given by the orthogonal projection of $\boldsymbol{\tau}$ on **s,** τ_s can be negative. Three cases are shown, with the same shear stress modulus (τ): (a) small angle α, close vectors $\boldsymbol{\tau}_s$ and $\boldsymbol{\tau}$, SSSC value τ_s close to τ; (b) angle α close to 90° small SSSC value; (b) large obtuse angle α, close vectors $\boldsymbol{\tau}_s$ and $\boldsymbol{\tau}$, SSSC value τ_s negative and close to $-\tau$. The misfit continuously increases while α varies from 0 to 180°.

Geological analyses have revealed that slip occurs on some faults despite a large angle between the slip vector and the shear stress as a consequence of geometrical requirements in faulted block patterns, a situation that is confirmed by modelling (Dupin *et al.* 1993). For this reason, it is preferable to consider that the parallelism between the shear stress and the slip is favourable but not compulsory. If large enough, the shear stress can induce fault slip along directions oblique to the shear stress vector. By definition (Fig. 1), the SSSC value is proportional to the shear stress for a given angle α. Adopting this value as a criterion in stress-slip relationships thus implies that the calculated shear stress should be large enough to induce fault motion along the direction of the actual slip, despite cohesion and friction. This is a different assumption compared with the Wallace–Bott hypothesis. Based on this hypothesis, the slip is simply expected to occur in the direction and sense of shear stress (Wallace 1951; Bott 1959). The conditions taking the shear stress magnitude into account were introduced in the inversion by Angelier (1984).

For acute shear slip-shear angles, maximizing the SSSC value includes an implicit requirement for the shear stress to be large: the larger the shear stress, the larger the SSSC. For obtuse angles, the SSSC is negative and its absolute value increases with shear stress, which accounts for the increasing difficulty in explaining the slip by stress. Thus, the algebraic SSSC value continuously increases with the shear stress. Simply considering the shear stress magnitude would be inappropriate, because a large shear stress with an obtuse shear slip-shear angle fails to explain the slip (Fig. 2c). On the other hand, even a zero-angle α cannot account for the slip if the shear stress is too small to activate the fault. The SSSC value, which combines the two aspects, is thus adopted herein as a key factor influencing the occurrence of fault slip. In more detail, the lower limit of τ_s for slip to occur depends on the normal stress and the coefficient of friction through Mohr–Coulomb-type relationships, an aspect analysed in Section 4 of this paper.

3 INVARIANCE OF THE SSSC VALUE FOR A DOUBLE COUPLE FOCAL MECHANISM

The case of double couple focal mechanisms of earthquakes is the primary target of the inverse problem addressed in this paper. For this reason, one must take into account the specific ambiguity of these mechanisms as compared with geological fault slips, that is, the existence of two, mutually exclusive, fault slips. Two nodal planes are perpendicular, and for each plane the potential slip vector is parallel to the normal of the other plane. Only one of the two possible slip vectors is the actual slip vector (Fig. 3)—it is often unknown which nodal plane is the fault. This is a major restriction within the framework of the Wallace–Bott hypothesis (that is, the parallelism between the shear stress and the fault slip). Assuming that a given nodal plane is the fault does not imply that the theoretical shear

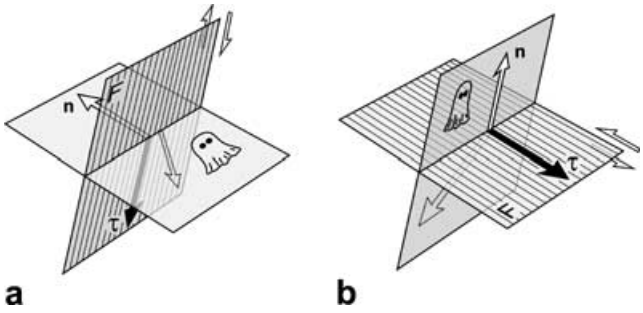

Figure 3. The intrinsic ambiguity of the double couple focal mechanism of an earthquake. The nodal planes are the same in (a) and (b), but the plane acting as fault differs. In both cases, the active nodal plane, F, is shown with striations parallel to slip and the shear sense is shown by a couple of open arrows. The other nodal plane is inactive and indicated by a ghost. Normal to actual fault as **n** (open arrow, solid line), shear stress on actual fault as $\boldsymbol{\tau}$ (black arrow). Calculated shear stress on inactive nodal plane as open dotted arrow. Actual slip and shear stress on fault plane are perpendicular to inactive nodal plane, but calculated shear stress on inactive nodal plane may be oblique to the fault plane. Note that (a) and (b) are mutually exclusive.

stress exerted virtually on the other (auxiliary) nodal plane should be perpendicular to the fault plane: it may be oblique as well (Fig. 3). Thus, one cannot consider that the Wallace–Bott hypothesis is valid for the two nodal planes simultaneously. It has been demonstrated (Angelier 1984) that such an assumption would imply

$$n_1 n_2 n_3 \Phi (1 - \Phi) = 0, \tag{1}$$

where n_1, n_2 and n_3 are the direction cosines of the normal to one of the nodal planes in the system of the principal stress axes, while Φ is the ratio between the principal stress differences expressed as follows (Angelier 1975):

$$\Phi = \frac{\sigma_2 - \sigma_3}{\sigma_1 - \sigma_3}. \tag{2}$$

Eq. (1) shows that except in particular cases a stress tensor does not simultaneously account for the two possible fault movements of an earthquake mechanism. The first type of exception, with n_1, n_2 or n_3 being zero, refers to nodal planes containing a principal stress axis. This is the case for the mechanisms that belong to conjugate fault patterns in the sense of Anderson (1942). The second type of exception, with Φ reaching one of its bound values, 0 or 1, concerns particular stress states with two principal stresses being equal. It was illustrated through the inversion of a set of microearthquakes by Angelier (1984).

The potential for fault slip to occur on each of the nodal planes, adopting the simplifying assumption of homogeneous stress, depends on the modulus, τ_s, of the slip component of the shear stress, which may act on this plane as a function of the stress regime. This modulus is the same for both the nodal planes, so that the determination of the SSSC value does not require any choice between them. Taking advantage of the lack of dependence of the SSSC modulus on the choice between nodal planes is worthwhile in the stress inversion of double couple focal mechanisms of earthquakes. This essential property deserves a demonstration as follows.

Let us consider the two perpendicular unit normal vectors, $\mathbf{n}_1$ and $\mathbf{n}_2$, describing the two nodal planes, F_1 and F_2, of the double couple mechanism (Fig. 4). The index numbers 1 and 2 are arbitrary. The stress tensor is $\boldsymbol{T}$ and the stress vector exerted on the nodal plane F_i is $\boldsymbol{T}\mathbf{n}_i$. The SSSC vector, $\boldsymbol{\tau}_{si}$, is the projection of this stress vector on the potential slip-parallel vector, $\mathbf{s}_i$ (Fig. 1). Thus, the SSSC values, τ_{s1} and τ_{s2}, for the two nodal planes, are given by

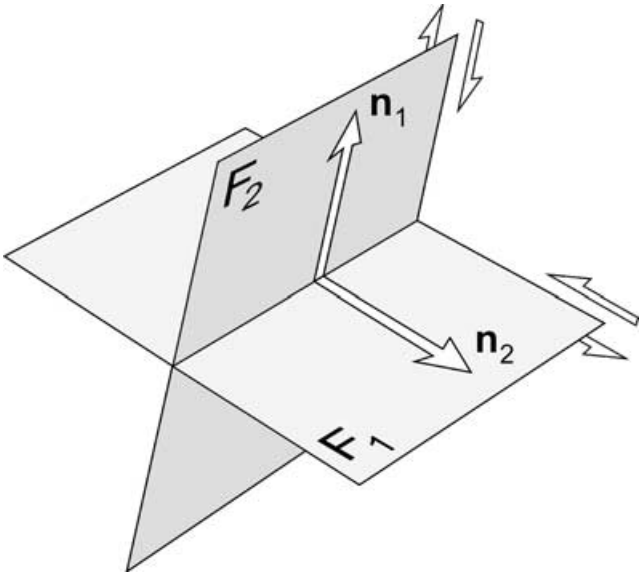

Figure 4. Perpendicular nodal planes (F_1 and F_2) and normal unit vectors ($\mathbf{n}_1$ and $\mathbf{n}_2$) of a double couple focal earthquake mechanism. Permitted shear senses shown by couples of open arrows. Compare with Fig. 3. See eqs (3) and (4).

$$\tau_{s1} = (\boldsymbol{T}\mathbf{n}_1) \cdot \mathbf{s}_1 \quad \text{and} \quad \tau_{s2} = (\boldsymbol{T}\mathbf{n}_2) \cdot \mathbf{s}_2, \tag{3}$$

where the dot denotes the scalar product. If slip occurs on the nodal plane F_1, the slip-parallel unit vector, $\mathbf{s}_1$, is perpendicular to F_2, so that $\mathbf{s}_2$ and $\mathbf{n}_1$ are identical. If slip occurs on F_2, the slip-parallel unit vector, $\mathbf{s}_2$, is perpendicular to F_1, so that $\mathbf{s}_1$ and $\mathbf{n}_2$ are identical. Consequently, the expressions (3) of the SSSC values for planes F_1 and F_2 can be written as follows:

$$\tau_{s1} = (\boldsymbol{T}\mathbf{n}_1) \cdot \mathbf{n}_2 \quad \text{and} \quad \tau_{s2} = (\boldsymbol{T}\mathbf{n}_2) \cdot \mathbf{n}_1. \tag{4}$$

Because of the distributive properties of the products, the two expressions (4) are identical. This shows that given a stress state and a double couple focal mechanism, a single SSSC value, τ_s, exists regardless of the nodal plane acting as the fault. This value can be determined by a simple consideration of the stress tensor, $\boldsymbol{T}$, and the two unit vectors that describe the focal mechanism, $\mathbf{n}_1$ and $\mathbf{n}_2$ (Fig. 4), as eq. (4) shows. Reciprocally, the determination of the slip component of the shear stress (τ_s, the SSSC value) does not require any choice between the two nodal planes.

This property is exploited in the subsequent mechanical analysis. Note that it is valid in terms of the SSSC value, but not in terms of SSSC vectors. Note also that only one of the two nodal planes is the actual fault. Its slip vector is perpendicular to the other nodal plane, but the shear stress that would theoretically act on this other nodal plane has no reason to be perpendicular to the fault plane: it may be oblique. This alternative shear stress geometry (Fig. 3) is crucial in the inversion of double couple mechanisms, and justifies the use of the SSSC value.

4 MECHANICAL SIGNIFICANCE OF THE SSSC

The expression of the SSSC value, τ_s, given in eqs (3) can be written in a different manner, as a function of the modulus of the shear stress, τ, and the slip-shear angle, α (Fig. 1). For both τ and α different values may be determined depending on the nodal plane considered,

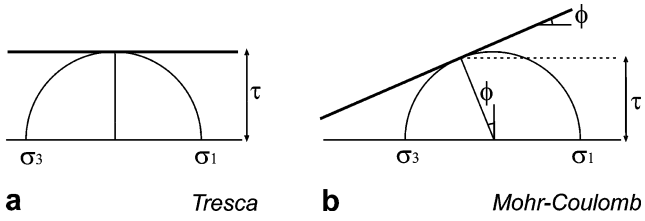

Figure 5. Tresca (a) and Mohr–Coulomb (b) criteria for failure, in Mohr's diagrams with normal stress (σ) as abscissas and shear stress (τ) as ordinates. The friction angle is φ.

although the SSSC value is unique regardless of this choice. This dependence is shown by the presence of the index i (1 or 2, the number of the nodal plane) on the right-hand side of the following expression:

$$\tau_s = \tau_i \cos \alpha_i . \quad (5)$$

This expression highlights the significance of the SSSC value as the product of two terms: a stress and the cosine of an angle. The latter factor, cos α, decreases from 1 to -1 as the slip-shear angle increases from 0° to 180° (Fig. 2). The largest value, 1, corresponds to the ideal case of a fault moving in the direction and sense of the shear stress. A zero value indicates a slip perpendicular to the shear stress. The lowest value, -1, corresponds to a fault moving in the direction opposite to the shear stress. As a result, this factor, cos α, should be made algebraically as large as possible in the inversion process: the value 1 means that the focal mechanism solution perfectly fulfils the Wallace–Bott requirement, whereas the value -1 reveals total inconsistency.

The other factor, τ, has often been ignored in stress inversion methods, although it plays an important role because slip is generally unlikely to occur for very low shear stress (see the discussion in Angelier 1990). This magnitude of shear stress is by essence positive and ranges between 0 and a maximum value, τ_{max}. A zero value implies that no slip occurs on the fault because the stress vector, $\boldsymbol{\sigma}$, must be null or perpendicular to the fault plane. The largest possible shear stress modulus, τ_{max}, depends on the stress tensor and equals half the differential stress, $\sigma_1 - \sigma_3$ (Fig. 5).

The occurrence of slip depends on the relationship between the normal and tangential components of stress through a friction coefficient, as formulated in the Mohr–Coulomb law. Interesting attempts have been made to account for these aspects (Reches 1987). In the inverse approach, it is, however, difficult to quantify the friction coefficient in a rigorous way, because it may vary widely within the data set depending on fault properties, and is generally unknown anyway. Introducing the explicit Mohr–Coulomb criterion in the inversion process is not difficult, but imposes numerical resolution of the problem. This limitation exists because inequalities are involved, which precludes the simple analytical solutions proposed in the present paper. Because of its crucial role in the occurrence of slip as a function of stress, the shear stress magnitude should be considered in some way, rather than being neglected.

The mechanical meaning of the SSSC can be illustrated with simple situations. For instance, with a uniaxial compressive stress (e.g. $\sigma_3 = \sigma_2$, hence $\Phi = 0$), the failure planes optimally tangent cones at a 45° angle about the stress axis σ_1, and the projection of σ_1 on these planes is the ideal slip vector. With a pure biaxial stress (e.g. $\sigma_1 + \sigma_3 = 0$ while $\sigma_2 = 0$, hence $\Phi = 0.5$), the two optimal failure planes contain the σ_2 axis and make angles of 45° with the other axes, the ideal slip vector being the projection of σ_1 on these planes. In such particular cases, both τ and τ_s are maximum (τ_{max}). Having the SSSC as large as possible is thus reasonable to reconstruct a stress state that accounts for the observed slips. One observes that this approach is underlain by the Tresca criterion (Fig. 5a), not by the Mohr–Coulomb criterion (Fig. 5b). The Tresca criterion may account poorly, in a theoretical way, for the activation of pre-existing discontinuities with various orientations. The SSSC is used as an approximation of the Mohr–Coulomb criterion.

This approximation is, however, justified in practice, for three main reasons. First, in the most common cases, the points of the Mohr diagram that correspond to fault activation are located near the top of the Mohr circle, that is, at relatively high levels of shear stress; in such situations, the difference is small. For an angle φ of 30° corresponding to a friction coefficient of about 0.6 (a common value), the difference between the two criteria represents only 13 per cent of the maximum shear stress (Fig. 5). The second practical reason is drastic considering the data available in actual situations. Not only would the adoption of the Mohr–Coulomb criterion require the choice between nodal planes (because the equivalence between the two planes, as demonstrated in Section 3, would disappear), it would also become compulsory to give values to unknown or very poorly constrained parameters. Typical parameters, in this respect, are friction coefficients or fluid pressures. The third reason lies in the major role played by the orientation parameters in the inversion. Numerical simulations reveal that with data sets showing a large variety of nodal plane attitudes, and aiming to obtain SSSC values as large as possible, the geometrical constraints related to α values are very strong compared with those related to τ values. This is not the case for data sets with little variety in nodal plane orientation.

Thus, using the SSSC criterion should be regarded as a reasonable approximation and a compromise between the adoption of a rigorous Mohr–Coulomb criterion (which is extremely difficult in practice because of unknown parameters), and the consideration of the sole angle α (meaning that fault activation does not depend on shear stress). Concerning fault slip data, how the friction is considered in stress inversion is a crucial problem. This problem has been addressed while comparing inversion methods that represent end-members views in that respect (Angelier 1991): two 4-D search inversion methods, in which friction is by definition ignored, and the so-called direct inversion method, in which it plays a large, albeit qualitative, role.

5 MAXIMIZING THE SSSC TO FIND THE BEST-FITTING STRESS TENSOR

As a consequence of the variations in the two factors on the right-hand side of eq. (5), a set of shear data that is well accounted for by stress is expected to display statistically high algebraic values of the SSSC. This is because both τ and cos α increase as the misfit decreases. It is thus proposed, in this paper, to search for the largest possible value of τ_s within a set of K mechanisms. In other words, one aims to find the stress tensor that corresponds to the largest average SSSC value. The extreme possible values of the SSSC are $-\tau_{max}$ and τ_{max} (as noted in Section 4, τ_{max} is the largest possible shear stress with the stress tensor). These bounds, respectively, correspond to the best fit and the largest misfit with the stress state considered. They are obtained for particular planes, which are parallel to the intermediate stress axis, $\boldsymbol{\sigma}_2$, and make angles of 45° with the extreme stress axes, $\boldsymbol{\sigma}_1$ and $\boldsymbol{\sigma}_3$. This attitude implies a value of τ_{max} for the shear stress, τ. Depending on the sense of shear, this also implies values of τ_{max} or $-\tau_{max}$ for τ_s, respectively indicating a perfect fit and total inconsistency with respect to the SSSC criterion.

The search for the maximum value of τ_s must be done for all the mechanisms of the data set simultaneously. It is performed through an analytical determination of the extrema of the sum of SSSC values, hereafter called *S*. To find the largest sum, this determination is followed by the selection of the algebraically largest extremum among the few solutions. Because the misfit criterion only depends on the SSSC values, this strategy is especially appropriate for analysing sets of double couple focal mechanisms of earthquakes, as it does not require any choice between the nodal planes. According to this principle, the simplest function *S* to consider is

$$S = \sum_{k=1}^{k=K} \tau_{sk}, \tag{6}$$

where *K* is the number of data points. According to this definition, *S* is the sum of SSSC values and may range from $-K\tau_{max}$ to $K\tau_{max}$. Consequently, the maximization of *S* is not carried out in the least-squares sense. To fulfil such a requirement, one may adopt the function S':

$$S' = \sum_{k=1}^{k=K} (\tau_{max} - \tau_{sk})^2, \tag{7}$$

where $(\tau_{max} - \tau_{sk})^2$ ranges from 0 (the best possible fit) to $4\tau_{max}^2$ (the largest possible misfit). As a result, S' may range from 0 to $4K\tau_{max}^2$. Using this criterion, one aims to minimize S' (instead of maximizing *S*), and the inversion is performed in a least-squares sense.

In practice, attempts at using the definition (7) to solve the inverse problem were less successful than those based on the definition (6), because they give too much weight to the anomalous values. This is a serious concern because many natural data sets show low levels of homogeneity; they often include erroneous or inaccurate individual determinations, as well as mechanisms that reflect different states of stress. By definition, a solution obtained with a least-squares approach shows more sensitivity to large misfits than one based on a lower degree function. This explains why the inversion based on eq. (7) may lack stability when the proportion of large misfits exceeds the reasonable levels predicted by a Gaussian-like distribution. The most robust inversion procedure was obtained based on the use of eq. (6), and hence was adopted.

6 *A PRIORI* AND *A POSTERIORI* PARAMETERS

The distinction between *a priori* and *a posteriori* parameters is crucial in inverse problems. It has been shown in Section 3, based on eqs (3) and (4), that the use of the SSSC value is appropriate because no *a priori* choice between nodal planes is required in the inversion. This does not contradict the *a posteriori* choice between the nodal planes to determine a 'preferred' fault slip. In Section 12 of this paper, the inversion and a review of an actual data set show that the *a posteriori* SSSC components, τ and α, may differ markedly for the two nodal planes of a single focal mechanism. This difference occurs because the *a posteriori* calculated shear stress vectors are often oblique to the intersection of the nodal planes (Fig. 6). This observation may seem surprising, remembering that a unique value of the SSSC was assumed prior to the inversion.

The paradox is apparent, not real. The SSSC value is unique for the *a priori* definition of the mechanism, which is assumed to fit the stress tensor perfectly: that is, the slip on the fault should be parallel to the shear stress (Fig. 6a). This condition implies identity between $\boldsymbol{\tau}$ and $\boldsymbol{\tau}_s$. In contrast, residual misfits exist in the *a posteriori* configuration, so that the slip and shear stress directions may differ (Fig. 6b). Note also that in the general case eq. (1) is not verified, so that the perfect situation shown in Fig. 6(a) cannot concern the two nodal planes at the same time (Fig. 3).

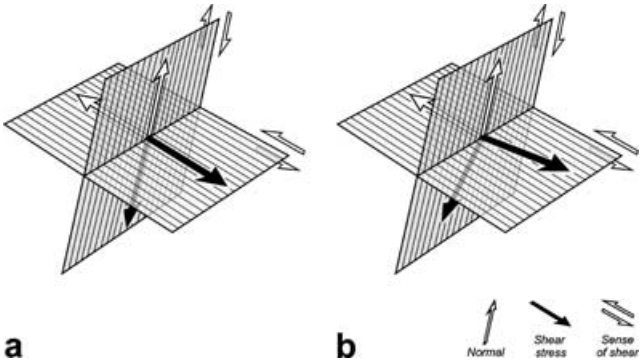

Figure 6. *A priori* (a) and *a posteriori* (b) configurations in the inverse problem. Nodal planes shown with thin lines parallel to potential slip vectors (mutually exclusive, see Fig. 3). Shear senses as couples of small arrows. Normal to the fault planes as open arrows, shear stresses as black arrows. The shear stress is parallel to slip according to the *a priori* model (a), but may be oblique in the *a posteriori* configuration as a consequence, of residual misfits (b).

Concerning the inversion of geological fault slip data, which are also subject to residual misfits, the above considerations concerning *a priori* and *a posteriori* parameters are valid, but there is no duality of the *a posteriori* parameters. For a double couple focal mechanism for an earthquake, this duality results from two factors. The first factor is the residual misfit that commonly exists for each focal mechanism after the best-fitting solution has been found for the whole data set. The second factor lies in the intrinsic ambiguity of focal mechanisms (Fig. 3). Both of these factors concur to produce an *a posteriori* situation with different slip-shear angles α and shear stress magnitudes τ (Fig. 6b). This aspect is illustrated numerically in Section 12.

The choice between nodal planes may follow the new SSSC-based inversion as a final step, but is not indispensable. Geological or geophysical reasons may support the choice of a nodal plane, such as a fault attitude revealed by geological mapping or an alignment of aftershocks revealed by seismological records. If such information is not available, the selection of a nodal plane can be made according to consideration of the slip-shear angle and the shear stress, the two factors distinguished in eq. (5). This choice is made *a posteriori*, and thus does not influence the result of the inversion accomplished before. In this respect, the approach proposed in this paper differs drastically from those involving an *a priori* choice, which affects the inversion. It also differs from the approach involving simultaneous inversion and nodal plane selection. In this case, not only does the choice affect the result, but also a bias is introduced in the algorithm: the process retains the nodal plane that best fits the stress tensor that is being searched for, and thus selects 'good' and 'bad' data in a somewhat circular way.

Two mutually exclusive *a posteriori* situations are displayed for each mechanism (Fig. 3). Thus, for a data set of *N* mechanisms, there are 2^N possible sets of *a posteriori* parameters. Because of the misfits, the situations involve different shear stresses and different shear-slip angles (Fig. 6b). In practice, however, the difference between the *a posteriori* parameters obtained for the two nodal planes of a focal mechanism often falls in the range of uncertainties. This occurs, for instance, if the intersection between the nodal planes contains (or is close to) a principal stress axis, because the

expression on the left-hand side of eq. (1) is zero (or small). In nature, focal mechanisms with nodal planes that contain (or are close to) the intermediate stress axis, $\boldsymbol{\sigma}_2$, are not exceptional because conjugate (or nearly conjugate) faulting often occurs. The difference between *a posteriori* parameters is also small if two principal stresses are equal (or nearly equal) so that Φ equals (or approaches) 0 or 1, the expression on the left-hand side of eq. (1) being zero (or small). Such situations of revolution stress ellipsoid are less common than conjugate fault patterns. In other cases, differences between *a posteriori* parameters may occur, especially for mechanisms with nodal planes at contrasting angles with principal stress axes.

It has been shown that in the inversion to determine the average stress tensor, the adoption of a criterion based on the SSSC value, as in eqs (6) and (7), does not require identification of the nodal plane acting as a fault. The new inversion method enables one to simply ignore the choice between the nodal planes. This observation is of little interest for geologists, who observe the fault surface and the striations indicating the slip vector. However, for seismologists analysing double couple focal mechanisms of earthquakes, it is essential because of the ambiguity between the nodal planes (Fig. 3). This provided one of the main reasons to develop the new method.

7 THE EXPRESSION OF THE REDUCED STRESS TENSOR

The SSSC value depends on both the geometry of each datum and the common stress tensor. The stress tensor normally contains six independent variables. However, the direction and the sense of shear stress on any plane do not depend on two of these variables: a pressure (which does not influence the shear stress) and a scale factor (which simply modifies the magnitudes of all stress components in the same proportion). In other words, with $\boldsymbol{T}$ being the average stress tensor solution of the inverse problem, any tensor $k\boldsymbol{T} + l\mathbf{I}$ is also a solution of the problem, because it induces the same directions and sense of shear stress on any plane. Note that k is a positive (non-zero) scale factor, $l\mathbf{I}$ an isotropic stress (l is a pressure, positive or negative, and $\mathbf{I}$ is the unit matrix).

In essence, the earthquake data indicate that a fault slip has occurred. The most reliable information is the direction and sense of slip (a unique definition for faults, an alternative for focal mechanisms). Based on this information, the values of k and l cannot be determined. To go further and determine these two unknowns, additional information is needed, such as rupture and friction parameters, fluid pressure status and depth of overburden (Angelier 1989). Without this information, one considers a reduced stress tensor, with four unknowns instead of six. Three unknowns control the orientation of the principal stress axes, the third one is a function of the ratio between principal stress differences, Φ, defined in eq. (2). These four unknowns carry important information concerning the type and orientation of the state of stress (Fig. 7).

In this paper, the stress tensor, $\boldsymbol{T}$, is chosen under a general form with rigorous separation between the components related to the orientations of the three principal axes and those related to the principal stress magnitudes, σ_1, σ_2 and σ_3 ($\sigma_1 \geq \sigma_2 \geq \sigma_3$, pressure positive):

$$\begin{pmatrix} T_{11} & T_{21} & T_{31} \\ T_{12} & T_{22} & T_{32} \\ T_{13} & T_{23} & T_{33} \end{pmatrix} = \begin{pmatrix} x_1 & x_2 & x_3 \\ y_1 & y_2 & y_3 \\ z_1 & z_2 & z_3 \end{pmatrix} \cdot \begin{pmatrix} \sigma_1 & 0 & 0 \\ 0 & \sigma_2 & 0 \\ 0 & 0 & \sigma_3 \end{pmatrix} \cdot \begin{pmatrix} x_1 & y_1 & z_1 \\ x_2 & y_2 & z_2 \\ x_3 & y_3 & z_3 \end{pmatrix}. \quad (8)$$

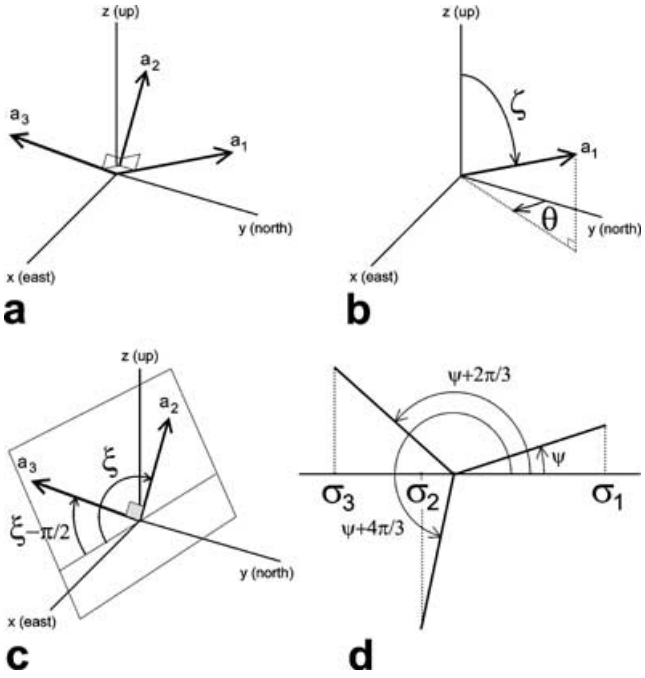

Figure 7. Reference frame (x-, y- and z-axes) and stress axes. (a) The system of principal stress axes are called $\mathbf{a}_1$, $\mathbf{a}_2$ and $\mathbf{a}_3$, rather than $\boldsymbol{\sigma}_1$, $\boldsymbol{\sigma}_2$ and $\boldsymbol{\sigma}_3$, because of switches related to ψ values. (b) Characterization of first axis, $\mathbf{a}_1$, with two angles, a trend (θ) and a plunge (ζ). (c) Characterization of second and third axes, $\mathbf{a}_2$ and $\mathbf{a}_3$, using a pitch (ξ) in the plane perpendicular to the first axis. (d) Relationship between the unknown ψ and the principal stresses.

On the right-hand side of eq. (8), the rotation matrix and the corresponding inverse matrix contain nine direction cosines, x_i, y_i and z_i ($i = 1, \ldots, 3$). These variables describe the orientations of the principal stress axes in the reference frame. The reference frame is constituted by the x-axis in the east direction, the y-axis in the north direction and the z-axis upward (Figs 7a–c). Because the nine direction cosines describe three perpendicular unit vectors, six relationships exist, which means that only three independent unknowns describe the orientations of principal stress axes. They will be made explicit later. The remaining three unknowns describe the three principal stress values. They are contained in the expression of the stress tensor in the system of the principal stress axes, which is isolated as the central term on the right-hand side of eq. (8).

This central term contains the principal stress values, σ_1, σ_2 and σ_3, which correspond to independent unknowns. Because neither an additional pressure nor a positive scale factor can affect the direction and sense of the shear stress on any plane, two unknowns cannot be determined with the sole directions and senses of shear stresses. As a result, the central term on the right-hand side of eq. (8) can be simplified as a function of a single variable. One possibility consists of adopting 1, β and $-1 - \beta$ as the three principal stress values, which shows that the trace is zero and that the absolute stress magnitudes cannot be found. Another possibility consists of adopting the following expression that also contains a single unknown, ψ (Angelier 1990):

$$\begin{pmatrix} \sigma_1 & 0 & 0 \\ 0 & \sigma_2 & 0 \\ 0 & 0 & \sigma_3 \end{pmatrix} = \begin{pmatrix} \cos\psi & 0 & 0 \\ 0 & \cos\left(\psi + \frac{2}{3}\pi\right) & 0 \\ 0 & 0 & \cos\left(\psi + \frac{4}{3}\pi\right) \end{pmatrix}. \quad (9)$$

This expression also implies that the trace is zero and that the stress scale is unknown, but an additional property is the constant sum of the squares of the principal stress values (this would not the case with 1, β and $-1-\beta$). Because of both this second invariant property and the geometrical significance of the angle ψ (Fig. 7d) which results in more elegant chains of equations, the expression (9) was adopted. Introducing this particular form in the general expression (8), one obtains a reduced stress tensor, with four independent unknowns instead of six. These four unknowns include three variables related to stress orientation and a single variable, ψ, related to magnitudes. Knowing that T_{ij} and T_{ji} are identical, one obtains the six different components of the stress tensor in the reference coordinate frame:

$$
\begin{aligned}
T_{11} &= x_1^2\cos\psi + x_2^2\cos\left(\psi+\frac{2\pi}{3}\right) + x_3^2\cos\left(\psi+\frac{4\pi}{3}\right)\\
T_{22} &= y_1^2\cos\psi + y_2^2\cos\left(\psi+\frac{2\pi}{3}\right) + y_3^2\cos\left(\psi+\frac{4\pi}{3}\right)\\
T_{33} &= z_1^2\cos\psi + z_2^2\cos\left(\psi+\frac{2\pi}{3}\right) + z_3^2\cos\left(\psi+\frac{4\pi}{3}\right)\\
T_{12} &= x_1y_1\cos\psi + x_2y_2\cos\left(\psi+\frac{2\pi}{3}\right) + x_3y_3\cos\left(\psi+\frac{4\pi}{3}\right)\\
T_{23} &= y_1z_1\cos\psi + y_2z_2\cos\left(\psi+\frac{2\pi}{3}\right) + y_3z_3\cos\left(\psi+\frac{4\pi}{3}\right)\\
T_{31} &= z_1x_1\cos\psi + z_2x_2\cos\left(\psi+\frac{2\pi}{3}\right) + z_3x_3\cos\left(\psi+4\frac{4\pi}{3}\right).
\end{aligned}
\tag{10}
$$

Because it is aimed at solving the problem analytically, it is indispensable to express these components of the stress tensor as explicit functions of the four independent variables contained in this tensor. This is done in the following equations. First, the six eqs (10) can be written as functions of $\cos\psi$ and $\sin\psi$:

$$
\begin{aligned}
T_{11} &= \frac{1}{2}\left(2x_1^2-x_2^2-x_3^2\right)\cos\psi + \frac{\sqrt{3}}{2}\left(x_3^2-x_2^2\right)\sin\psi\\
T_{22} &= \frac{1}{2}\left(2y_1^2-y_2^2-y_3^2\right)\cos\psi + \frac{\sqrt{3}}{2}\left(y_3^2-y_2^2\right)\sin\psi\\
T_{33} &= \frac{1}{2}\left(2z_1^2-z_2^2-z_3^2\right)\cos\psi + \frac{\sqrt{3}}{2}\left(z_3^2-z_2^2\right)\sin\psi\\
T_{12} &= \frac{1}{2}\left(2x_1y_1-x_2y_2-x_3y_3\right)\cos\psi + \frac{\sqrt{3}}{2}\left(x_3y_3-x_2y_2\right)\sin\psi\\
T_{23} &= \frac{1}{2}\left(2y_1z_1-y_2z_2-y_3z_3\right)\cos\psi + \frac{\sqrt{3}}{2}\left(y_3z_3-y_2z_2\right)\sin\psi\\
T_{31} &= \frac{1}{2}\left(2z_1x_1-z_2x_2-z_3x_3\right)\cos\psi + \frac{\sqrt{3}}{2}\left(z_3x_3-z_2x_2\right)\sin\psi.
\end{aligned}
\tag{11}
$$

The coordinates x_i, y_i and z_i ($i=1,\ldots,3$) are functions of three independent variables, chosen as three angles, θ, ζ and ξ defined in a quasi-Eulerian way (Fig. 7). Note that the principal stresses have been labelled in a definite algebraic order ($\sigma_1\geq\sigma_2\geq\sigma_3$). However, according to eq. (9), this order may change depending on ψ, which conflicts with the definition; in other words, switches may occur between principal stress axes (Fig. 7d). For this reason, the principal axes shown in Fig. 7(a) are labelled $\mathbf{a}_1$, $\mathbf{a}_2$ and $\mathbf{a}_3$, instead of $\boldsymbol{\sigma}_1$, $\boldsymbol{\sigma}_2$ and $\boldsymbol{\sigma}_3$. Otherwise, using expression (9) would induce mistakes because maintaining $\sigma_1\geq\sigma_2\geq\sigma_3$ would impose a restriction on ψ.

The first axis, $\mathbf{a}_1$, is characterized by two angles (Fig. 7b): its trend, θ, and its angle, ζ, with the z-axis (up). In the reference frame (Fig. 7a), the direction cosines for this axis are

$$
\begin{aligned}
x_1 &= \sin\theta\sin\zeta\\
y_1 &= \cos\theta\sin\zeta\\
z_1 &= \cos\zeta.
\end{aligned}
\tag{12}
$$

An angle ξ allows characterization of the second axis, $\mathbf{a}_2$. This angle is a pitch in the plane perpendicular to $\mathbf{a}_1$, counted clockwise from the left-hand side (Fig. 7c). One thus obtains

$$
\begin{aligned}
x_2 &= \cos\theta\cos\xi - \sin\theta\cos\zeta\sin\xi\\
y_2 &= -\sin\theta\cos\xi - \cos\theta\cos\zeta\sin\xi\\
z_2 &= \sin\zeta\sin\xi.
\end{aligned}
\tag{13}
$$

Removing a right angle to the pitch, one obtains the direction cosines for the third axis, $\mathbf{a}_3$:

$$
\begin{aligned}
x_3 &= \cos\theta\sin\xi + \sin\theta\cos\zeta\cos\xi\\
y_3 &= -\sin\theta\sin\xi + \cos\theta\cos\zeta\cos\xi\\
z_3 &= -\sin\zeta\cos\xi.
\end{aligned}
\tag{14}
$$

Substituting into eq. (11) the expressions of the direction cosines from eqs (12)–(14), one obtains the components of the stress tensor as functions of four independent unknowns, the angles θ, ζ, ξ and ψ. The diagonal components, T_{ii}, of the stress tensor are:

$$
\begin{aligned}
T_{11} &= \frac{3}{2}\left(\sin^2\theta\sin^2\zeta-\frac{1}{3}\right)\cos\psi\\
&\quad -\frac{\sqrt{3}}{2}\left[\left(\sin^2\theta\sin^2\zeta+\cos2\theta\right)\cos2\xi\right.\\
&\quad \left.-\sin2\theta\cos\zeta\sin2\xi\right]\sin\psi\\
T_{22} &= \frac{3}{2}\left(\cos^2\theta\sin^2\zeta-\frac{1}{3}\right)\cos\psi\\
&\quad -\frac{\sqrt{3}}{2}\left[\left(\cos^2\theta\sin^2\zeta-\cos2\theta\right)\cos2\xi\right.\\
&\quad \left.+\sin2\theta\cos\zeta\sin2\xi\right]\sin\psi\\
T_{33} &= \frac{3}{2}\left(\cos^2\zeta-\frac{1}{3}\right)\cos\psi + \frac{\sqrt{3}}{2}\sin^2\zeta\cos2\xi\sin\psi,
\end{aligned}
\tag{15}
$$

while the other components, $T_{ij}=T_{ji}$, are given by

$$
\begin{aligned}
T_{12} &= \frac{3}{4}\sin2\theta\sin^2\zeta\cos\psi\\
&\quad +\frac{\sqrt{3}}{4}\left[\sin2\theta\left(2-\sin^2\zeta\right)\cos2\xi+2\cos2\theta\cos\zeta\sin2\xi\right]\sin\psi\\
T_{23} &= \frac{3}{4}\cos\theta\sin2\zeta\cos\psi\\
&\quad -\frac{\sqrt{3}}{4}\left[\cos\theta\sin2\zeta\cos2\xi-2\sin\theta\sin\zeta\sin2\xi\right]\sin\psi\\
T_{31} &= \frac{3}{4}\sin\theta\sin2\zeta\cos\psi\\
&\quad -\frac{\sqrt{3}}{4}\left[\sin\theta\sin2\zeta\cos2\xi+2\cos\theta\sin\zeta\sin2\xi\right]\sin\psi.
\end{aligned}
\tag{16}
$$

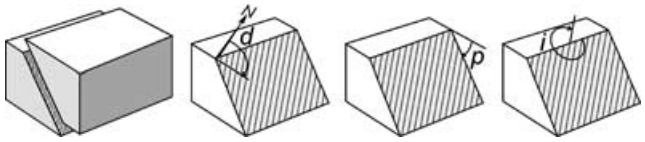

Figure 8. The basic datum. The block diagram illustrates the fault slip geometry (in this case, a reverse left-lateral fault). The three angles are d, dip direction of fault (azimuth); p, fault dip angle; i, pitch of slip. By convention the pitch is counted clockwise from the right-hand side of the fault. A pitch between 0° and 90° indicates normal left-lateral slip, a pitch between 90° and 180° indicates normal right-lateral slip, a pitch between 180° and 270° indicates reverse right-lateral slip, and a pitch between 270° and 360° indicates reverse left-lateral slip. Pitches of 0° 90° 180° and 270° indicate pure left-lateral, normal, right-lateral and reverse slips, respectively.

8 THE EXPRESSION OF THE SSSC VALUE

In the reference frame already defined (Fig. 7), n_x, n_y and n_z define the unit vector, **n**, normal to the fault or nodal plane. Considering the original data, these direction cosines are calculated as functions of two angles, the dip direction of the plane, d, and the fault dip, p (Fig. 8):

$$\begin{aligned} n_x &= \sin d \sin p \\ n_y &= \cos d \sin p \\ n_z &= \cos p. \end{aligned} \tag{17}$$

With the stress tensor $\boldsymbol{T}$, the stress vector acting on this plane, $\boldsymbol{\sigma}$, is obtained as the product $\boldsymbol{T}\mathbf{n}$. The coordinates of $\boldsymbol{\sigma}$, σ_x, σ_y, and σ_z, are thus given by

$$\begin{pmatrix} \sigma_x \\ \sigma_y \\ \sigma_z \end{pmatrix} = \begin{pmatrix} T_{11} & T_{21} & T_{31} \\ T_{12} & T_{22} & T_{32} \\ T_{13} & T_{23} & T_{33} \end{pmatrix} \cdot \begin{pmatrix} n_x \\ n_y \\ n_z \end{pmatrix}. \tag{18}$$

In the same reference frame, s_x, s_y and s_z define the unit slip vector, **s**, perpendicular to **n** (Fig. 1). These direction cosines are functions of the original data. They depend on two angles, d and p, used in eq. (17) to define **n**, and also on the pitch of the slip vector, i (Fig. 8):

$$\begin{aligned} s_x &= \cos d \cos i - \sin d \cos p \sin i \\ s_y &= -\sin d \cos i - \cos d \cos p \sin i \\ s_z &= \sin p \sin i. \end{aligned} \tag{19}$$

As defined in an earlier section, the SSSC vector, $\boldsymbol{\tau}_\mathbf{s}$, is the orthogonal projection of $\boldsymbol{\tau}$ or $\boldsymbol{\sigma}$ on the unit vector **s** (Fig. 1). The SSSC value, τ_s, is obtained as the scalar product $\boldsymbol{\sigma} \cdot \mathbf{s}$:

$$\tau_s = s_x\sigma_x + s_y\sigma_y + s_z\sigma_z. \tag{20}$$

Combining eqs (18) and (20), one obtains τ_s as a function of the stress tensor components:

$$\begin{aligned} \tau_s = {} & n_x s_x T_{11} + n_y s_y T_{22} + n_x s_x T_{33} + (n_x s_y + n_y s_x) T_{12} \\ & + (n_y s_z + n_z s_y) T_{23} + (n_z s_x + n_x s_z) T_{31}. \end{aligned} \tag{21}$$

The next step consists of substituting into eq. (21) the expressions of the stress tensor as functions of the four independent unknowns θ, ζ, ξ and ψ, given in eqs (15) and (16). One first obtains the following expression, where the three angles ζ, ξ and ψ are explicit:

$$\begin{aligned} \tau_s = {} & \left(\frac{3}{4}\cos\psi - \frac{\sqrt{3}}{4}\cos 2\xi \sin\psi \right) \\ & \times \left[\frac{1}{2}(w-e)(1-\cos 2\zeta) + t \sin 2\zeta \right] + \frac{\sqrt{3}}{2} w \cos 2\xi \sin\psi \\ & + \frac{\sqrt{3}}{2} \sin 2\xi \sin\psi \,(v\cos\zeta + u\sin\zeta) + \frac{1}{2} e \cos\psi. \end{aligned} \tag{22}$$

The four terms t, u, v and w of eq. (22) are functions of the remaining angle, θ:

$$\begin{aligned} t &= b\cos\theta + c\sin\theta \\ u &= b\sin\theta - c\cos\theta \\ v &= a\cos 2\theta - d\sin 2\theta \\ w &= a\sin 2\theta + d\cos 2\theta. \end{aligned} \tag{23}$$

The four parameters, a, b, c and d contained in eqs (23), as well as the parameter e used in eq. (22), depend on the direction cosines of **n** and **s**. These six direction cosines have been calculated as functions of the three angular parameters of the kth fault or the nodal plane, d_k, p_k and i_k (Fig. 8), according to eqs (17) and (19). The parameters, a, b, c and d (note that d is a calculated parameter, whereas d_k is an observed angle) have simple expressions:

$$\begin{aligned} a &= n_x s_y + n_y s_x \\ b &= n_y s_z + n_z s_y \\ c &= n_z s_x + n_x s_z \\ d &= n_y s_y + n_x s_x \\ e &= 3 n_z s_z. \end{aligned} \tag{24}$$

9 SUMMATION OF THE SSSC VALUES

The inverse method consists of finding the four variables θ, ζ, ξ and ψ of the reduced stress tensor so that the sum of the values of the shear stress slip components is made maximum for the data set considered. From expression (22) of τ_s, the sum S defined in eq. (6) is

$$\begin{aligned} S = {} & \left(\frac{3}{4}\cos\psi - \frac{\sqrt{3}}{4}\cos 2\xi \sin\psi \right) \left[\frac{1}{2}(W-E)(1-\cos 2\zeta) \right. \\ & \left. + T \sin 2\zeta \right] + \frac{\sqrt{3}}{2} W \cos 2\xi \sin\psi \\ & + \frac{\sqrt{3}}{2} \sin 2\xi \sin\psi (V\cos\zeta + U\sin\zeta) + \frac{1}{2} E \cos\psi, \end{aligned} \tag{25}$$

with T, U, V, W defined as simple functions of θ:

$$\begin{aligned} T &= B\cos\theta + C\sin\theta \\ U &= B\sin\theta - C\cos\theta \\ V &= A\cos 2\theta - D\sin 2\theta \\ W &= A\sin 2\theta + D\cos 2\theta. \end{aligned} \tag{26}$$

The variables T, U, V and W refer to functions of sums of data, whereas the variables t, u, v and w used in eqs (23) refer to corresponding functions of a single datum. Likewise, the parameters A, B, C, D, used in eq. (26), as well as E used in eq. (25), are the sums, for the set of K data, of the individual terms a, b, c, d and e of eqs (24):

$$
\begin{aligned}
A &= \sum_{k=1}^{k=K} (n_{xk}s_{yk} + n_{yk}s_{xk}) \\
B &= \sum_{k=1}^{k=K} (n_{yk}s_{zk} + n_{zk}s_{yk}) \\
C &= \sum_{k=1}^{k=K} (n_{zk}s_{xk} + n_{xk}s_{zk}) \\
D &= \sum_{k=1}^{k=K} (n_{yk}s_{yk} + n_{xk}s_{xk}) \\
E &= 3\sum_{k=1}^{k=K} n_{zk}s_{zk}.
\end{aligned} \tag{27}
$$

The sum that we aim to maximize is now explicitly written as a function of four independent variables, the unknowns θ, ζ, ξ and ψ, in eqs (25) and (26). The data are expressed through five parameters, A, B, C, D and E, calculated using eqs (27). Considering the original data, whether the direction cosines that define the unit vectors $\mathbf{n}_k$ and $\mathbf{s}_k$ ($k = 1, \ldots, K$) are obtained with eqs (17) and (19) or from other angular definitions, is a technical matter.

Note that the functions actually used in the inversion are slightly more complex than those shown in the equations starting from (6). The function, S, must be normalized according to the value of τ_{max}. In other words, one aims to maximize S/τ_{max}, rather than S. This is indispensable because τ_{max} is not a constant, but is a function of the angle ψ (Fig. 7d). As a result, a maximization process based on a simple consideration of S would favour particular values of ψ giving large values of τ_{max}. To avoid this bias, the version of S adopted in the derivations was

$$
S = \frac{1}{\tau_{max}} \sum_{k=1}^{k=K} \tau_{sk}. \tag{28}
$$

This modification provides an elegant way to combine the invariant properties of the stress tensor, defined in eqs (8) and (9) and discussed in Section 7, with the requirement for a constant maximum shear stress. The problem arose because a non-zero stress tensor cannot simultaneously have a zero trace ($\sigma_1 + \sigma_2 + \sigma_3$), a constant function $\sigma_1^2 + \sigma_2^2 + \sigma_3^2$ and a constant maximum shear stress $(\sigma_1 - \sigma_3)/2$. A similar problem was discussed in this journal, while presenting the direct inversion method (Angelier 1990). In the present case, it could be solved analytically at the cost of some transformations related to the variable ψ.

10 SEARCH FOR THE SMALLEST MISFIT

With the method adopted herein, the smallest average misfit corresponds to the largest average value of the SSSC, that is, the maximum value of S. One consequently tries to find the values of the four independent variables θ, ζ, ξ and ψ of the stress tensor, which result in the largest sum S defined in eq. (28). This search is done with the numerical values of parameters A, B, C, D and E listed in eqs (27). These five values depend on the geometrical characteristics of the K couples of perpendicular unit vectors, $\mathbf{n}_k$ and $\mathbf{s}_k$, of the data set. The only way to ensure fast resolution consists of solving a system of equations that sets to zero the four partial derivatives of S with respect to θ, ζ, ξ and ψ. One then determines the largest value among the few extrema of S. The partial derivatives of S are obtained from eqs (25) and (26):

$$
\begin{aligned}
\frac{\partial S}{\partial \psi} &= \left(-\frac{3}{4}\sin\psi - \frac{\sqrt{3}}{4}\cos 2\xi \cos\psi\right)\left[\frac{1}{2}(W-E)(1-\cos 2\zeta)\right. \\
&\quad \left. + T\sin 2\zeta\right] + \frac{\sqrt{3}}{2} W \cos 2\xi \cos\psi \\
&\quad + \frac{\sqrt{3}}{2}\sin 2\xi \cos\psi\,(V\cos\zeta + U\sin\zeta) - \frac{1}{2}E\cos\psi \\
\frac{\partial S}{\partial \xi} &= \frac{\sqrt{3}}{2}\sin 2\xi \sin\psi\left[\frac{1}{2}(W-E)(1-\cos 2\zeta) + T\sin 2\zeta\right] \\
&\quad - \sqrt{3}W\sin 2\xi \sin\psi + \sqrt{3}\cos 2\xi \sin\psi\,(V\cos\zeta + U\sin\zeta) \\
\frac{\partial S}{\partial \zeta} &= \left(\frac{3}{4}\cos\psi - \frac{\sqrt{3}}{4}\cos 2\xi \sin\psi\right)[(W-E)\sin 2\zeta \\
&\quad + 2T\cos 2\zeta] + \frac{\sqrt{3}}{2}\sin 2\xi \sin\psi\,(U\cos\zeta - V\sin\zeta) \\
\frac{\partial S}{\partial \theta} &= \left(\frac{3}{4}\cos\psi - \frac{\sqrt{3}}{4}\cos 2\xi \sin\psi\right)[V(1-\cos 2\zeta) \\
&\quad - U\sin 2\zeta] + \sqrt{3}V\cos 2\xi \sin\psi \\
&\quad + \frac{\sqrt{3}}{2}\sin 2\xi \sin\psi\,(T\sin\zeta - 2W\cos\zeta).
\end{aligned} \tag{29}
$$

To find the extrema of the function S defined in eq. (6), it suffices to solve the system of four equations cancelling the partial derivatives of S given in eqs (29) with respect to the four unknowns θ, ζ, ξ and ψ, as indicated below:

$$
\frac{\partial S}{\partial \psi} = 0, \quad \frac{\partial S}{\partial \xi} = 0, \quad \frac{\partial S}{\partial \zeta} = 0, \quad \frac{\partial S}{\partial \theta} = 0. \tag{30}
$$

This system of four equations could be solved by analytical means. A similar problem with different variables, equations and parameters was described in this journal (Angelier 1990). The present resolution follows the same guidelines but the equations are longer to write and difficult to present in an elegant way. It is possible to extract from the system of eqs (25) and (26) one equation with a single unknown. This equation is solved numerically and the solutions are introduced in the other equations, allowing determination of the three remaining variables.

Because several solutions are found, corresponding to minimum and maximum values of S, it is necessary to compare these solutions in order to find the maximum of S. A numerical comparison allows a quick identification of the largest value of S, and thus indicates the set of four variables θ, ζ, ξ and ψ that defines the reduced stress tensor solution of the inverse problem.

The inverse problem is solved with only four eqs (30). The intervention of the data is restricted to five parameters, listed in eqs (27). These simple sums are calculated once, prior to the inversion. Thus, the analytical resolution of the inverse problem proposed herein requires a constant—and negligible—computer runtime, regardless of the number of data. The only time difference between processing sets of 10 or 100 000 focal mechanisms of earthquakes is that needed to calculate the sums of eqs (27). As there is no need to store the data in memory, the space required by the program is small. For these reasons, the capacity of the inversion is unlimited in terms of the data set size.

In summary, the inversion process yields the reduced stress tensor that best accounts for the data set, based on the search for the largest possible sum of the SSSC values, as defined in eq. (28). The search for the best fit is performed through consideration of both

the orientation (including sense) of slip and the amplitude of the shear stress, the two factors made explicit in eq. (5). Thus, one obtains the smallest slip-shear angles and the largest possible shear stresses that can simultaneously exist for all the data taken together.

11 MAIN ESTIMATORS OF THE SSSC-BASED INVERSION

The slip-shear angle, α, is a well-known criterion in stress tensor determinations (Fig. 2). Having a shear stress, τ, as large as possible also makes sense, because the larger the shear stress, the higher the probability for slip to occur. This, however, is an approximation. A rigorous way to deal with stress magnitudes would require a Mohr–Coulomb-type criterion, and hence explicit consideration of the friction coefficient, the effective normal stress and the cohesion. This would involve a discontinuous function, because the probability for slip to occur reaches 1 for a certain value and cannot increase further (Fig. 5). Why this criterion was not used herein has been discussed in Section 4. Had it been adopted, arbitrary choices would have been necessary to define the friction coefficient, the cohesion and the fluid pressure (which affects the normal stress). These values should not even be considered uniform within a given data set, because they depend on factors that have no reason to be identical for all earthquakes, such as the shape of the fault surface, the fluid condition and the mechanical and permeability properties of fault gouges and host rocks. Such parameters (Angelier 1989) are generally unknown or poorly evaluated.

Applying a method controlled by so loosely constrained parameters is not desirable. It is certainly better to adopt as a first approximation a simple search for relatively large shear stress than to introduce arbitrary parameters. The approach adopted herein is also better than just taking the shear-slip angle into account, which would imply that the shear stress magnitude does not influence the occurrence of slip. The dual criterion underlying the use of the SSSC, presented in eq. (5) and Figs 1 and 2, is not the ultimate solution but is a reasonable compromise. Also, the SSSC-based inverse problem could be solved by analytical means, which would not have been possible with the discontinuous mathematical formulation of the Mohr–Coulomb criterion.

After the inversion, three main estimators enable one to evaluate the mechanical consistency of the data set, in terms of both the individual and the average misfit levels obtained with the best-fitting stress tensor (Fig. 9). Because the maximum shear stress amplitude, τ_{max}, depends on the stress tensor, the appropriate estimator for the SSSC value is not τ_s, but the ratio τ_s/τ_{max}. This normalized SSSC value, called ω, varies from -1 to 1, and increases algebraically as the misfit decreases (Fig. 9), consistent with the definition (28) of S. This fit estimator, omega (ω for a datum, ω_m as the average value), directly reflects the criterion used in the inversion. It is given as a percentage and thus ranges from -110 per cent (largest misfit) to 110 per cent (perfect fit).

For a more detailed analysis of the results of the inversion, one considers the two variables, τ and α, contained in the SSSC value (Figs 1 and 2). For the shear stress, τ, the appropriate estimator is the ratio τ/τ_{max}. This normalized shear stress is called τ^* and increases from 0 to 1 as the misfit decreases (Fig. 9). The first subsidiary estimator, tau (τ^* for a datum, τ_m^* as the average value), thus indicates the normalized shear stress level, as a percentage ranging

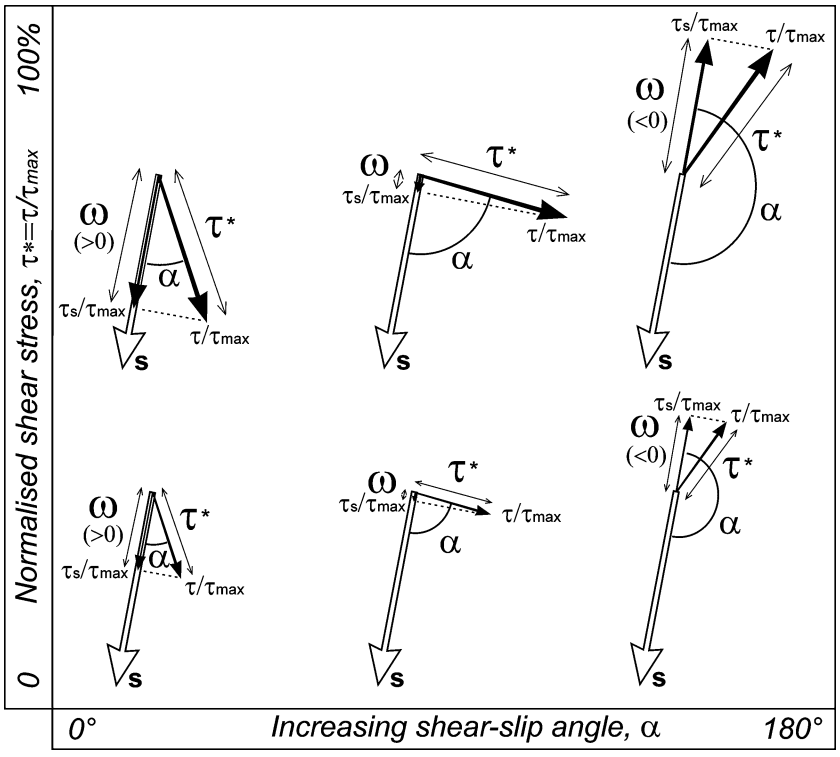

Figure 9. Definition of the three *a posteriori* estimators of the stress inversion, ω (omega), τ^* (tau) and α (ang), with examples of misfits for typical values of the latter two estimators. Unit slip vector as **s** (open arrow). Black arrows indicate the normalized shear stress vector, $\boldsymbol{\tau}/\tau_{max}$, and the normalized SSSC vector, $\boldsymbol{\tau}_s/\tau_{max}$. The two subsidiary estimators are tau, the normalized shear stress magnitude, $\tau^* = \tau/\tau_{max}$, from 0 to 100 per cent (ordinates), and ang, the shear-slip angle, α, from 0° to 180° (abscissas). The main estimator of the SSSC-based inversion is ω, from -100 to 100 per cent (negative if α is larger than 90° and positive otherwise). Note that the best possible fit would be found in the upper-left corner ($\alpha = 0°$ and $\tau = \tau_{max}$, so that $\omega = 100$ per cent), whereas the largest misfit would occur in the upper-right corner ($\alpha = 180°$ and $\tau = \tau_{max}$, so that $\omega = -100$ per cent).

from 0 per cent (no shear stress) to 110 per cent (maximum shear stress). Concerning the shear-slip angle, α, it varies from 0° to 180°, indicating increasing misfit. The second subsidiary estimator, ang (α for a datum, α_m as the average value), thus describes the shear-slip angle in degrees, from 0° (perfect fit) to 180° (largest misfit). The significance of these three estimators is illustrated in Fig. 9.

Because the method presented in this paper involves a very short runtime, there is no difficulty in including the stress inversion as a core in a variety of algorithms to refine or split the data set according to diverse rules. How the inversion can be included in an iterative process to split heterogeneous data sets into mechanically homogeneous subsets is beyond the scope of this study. An automatic separation process has already been used with other types of inversion (Angelier 1984), and can use the SSSC-based inversion as well. Even within single-phase data sets, data with large misfits are often present. Provided that valid reasons exist to reject these data, one can rule them out through an iterative process that involves series of SSSC-based inversions with increasing demand for good fits. The refining process allows one to obtain for a given initial data set a large number of stress states. The number of retained data decreases as the minimum acceptable fit level increases (ω_{acc}, the smallest acceptable value of ω).

The major interest of the refining process is twofold. First, it allows comparison with individual data uncertainties, in order to determine the level of data rejection that is most compatible with the data accuracy (large data uncertainties permit low ω_{acc}, whereas high data accuracy requires large ω_{acc}). Secondly, it enables one to evaluate the stability of the solutions of the stress inversion: the solution is stable if the stress state does not vary, or varies little, as ω_{acc} increases. Unstable solutions generally reveal mechanical heterogeneity of the data set. To evaluate the validity of the results, two parameters are essential: the number of rejected data and the largest acceptable misfit. They are more important than average misfits and standard deviations, which vary depending on the fit level requested and can be made small by choosing a severe fitting demand resulting in many rejected data (an artificial method of improving the inversion). Some specific parameters control the refining process. The choice of the smallest acceptable fit level for each step, ω_{acc}, depends on the accuracy and dispersion of the focal mechanisms (an auxiliary parameter is the variation of the fit level between two successive steps). The main estimator is the number of data rejected, N_R, as compared with the total number of data. The auxiliary estimator is the smallest individual fit within the retained data subset, ω_{min}.

12 APPLICATION WITH ACTUAL DATA

In this section, the application of the method to a set of focal mechanisms of earthquakes is discussed based on a typical example. Because the adoption of a large data set would preclude complete presentation of the inversion results, a limited number of data (116 mechanisms, i.e. 212 nodal planes) was retained. The data, the results and the individual misfits are displayed in Tables 1–3 , respectively. Consequently, the reader can carry out the inversion of the same data set with any other method, and compare the results.

A devastating earthquake occurred on 1999 September 20, in west-central Taiwan, killing more than 2400 inhabitants. This earthquake took place in the front zone of the fold-and-thrust belt of Taiwan (Fig. 10), and produced a nearly 110 km long surface rupture, most of it along a well-known west-verging thrust, the Chelungpu Fault. The energy magnitude of this Chichi earthquake was 7.6.

Table 1. Data set analysed in this paper. Focal mechanisms of 106 earthquakes of the Chichi sequence, 1999 September 20th to 2000 September 16th, determined by Kao & Chen (2000). For each focal mechanism, two nodal planes are given with arbitrary indices 1 and 2 following the earthquake index number (column 1). First format indicated by strike, dip and pitch, with letters indicating north (N), east (E), south (S) or west (W) and sense (s) of relative motion (S left-lateral, N normal, D right-lateral, I reverse). Second format based on the three angles of Fig. 7, *d* as fault dip direction, *p* as fault dip and *i* as pitch (conventions in the caption of Fig. 7).

Ref.	Strike	Dip	Pitch	s	*d*	*p*	*i*
168-1	147	35E	58S	I	57	35	302
168-2	4	61W	70S	I	274	61	250
169-1	23	32E	86N	I	113	32	266
169-2	18	58W	87N	I	288	58	273
170-1	123	49N	6E	S	33	49	354
170-2	29	85W	42S	D	299	85	222
171-1	155	38E	62S	I	65	38	298
171-2	9	57W	70S	I	279	57	250
172-1	159	63E	15S	S	69	63	345
172-2	62	77N	28W	D	332	77	208
173-1	167	24E	61S	N	77	24	119
173-2	18	69W	77S	N	288	69	77
174-1	66	48N	20E	D	336	48	160
174-2	142	75W	43S	S	232	75	43
175-1	173	52E	5N	S	83	52	5
175-2	86	86S	39W	D	176	86	141
176-1	10	37E	63S	I	100	37	297
176-2	43	58W	71S	I	313	58	251
177-1	104	17S	10W	D	194	17	170
177-2	4	87E	73N	N	94	87	73
178-1	154	41E	61S	I	64	41	299
178-2	10	55W	68S	I	280	55	248
179-1	155	54E	3S	S	65	54	357
179-2	63	88N	37W	D	333	88	217
180-1	98	53S	14W	D	188	53	166
180-2	179	79E	37N	S	89	79	37
181-1	25	30W	36N	S	295	30	324
181-2	83	73S	65E	I	173	73	245
182-1	83	13S	6E	D	173	13	186
182-2	179	89W	77N	I	269	89	283
183-1	175	45E	15N	S	85	45	15
183-2	96	79S	47W	N	186	79	133
184-1	159	44E	14N	S	69	44	14
184-2	79	80S	47W	N	169	80	133
185-1	124	49S	44W	D	214	49	136
185-2	2	58E	50N	N	92	58	50
186-1	164	42E	33N	S	74	42	33
186-2	100	69S	54W	N	190	69	126
187-1	23	61E	5N	S	113	61	5
187-2	115	86S	30W	D	205	86	150
188-1	23	37W	52N	I	293	37	308
188-2	67	62S	66E	I	157	62	246
189-1	113	37S	25W	D	203	37	155
189-2	3	75E	55N	N	93	75	55
190-1	169	60E	1N	S	79	60	1
190-2	80	89S	31W	D	170	89	149
191-1	156	44E	24S	S	66	44	336
191-2	48	74N	49W	I	318	74	229
192-1	177	44E	7S	S	87	44	353
192-2	82	85N	47W	I	352	85	227
193-1	81	76S	12W	D	171	76	168
193-2	168	78E	14N	S	78	78	14
194-1	165	76E	10S	S	75	76	350
194-2	73	80N	15W	D	343	80	195
195-1	101	22S	46E	I	191	22	226
195-2	55	74N	74E	I	325	74	286

Table 1. (*Continued.*)

Ref.	Strike	Dip	Pitch	s	*d*	*p*	*i*
196-1	93	71N	13W	D	3	71	193
196-2	7	78E	19S	S	97	78	341
198-1	167	36E	40S	S	77	36	320
198-2	43	68W	61S	I	313	68	241
199-1	131	53N	28E	S	41	53	332
199-2	23	68W	41S	D	293	68	221
200-1	162	62E	26N	S	72	62	26
200-2	85	67S	31W	D	175	67	149
201-1	89	36S	73E	I	179	36	253
201-2	68	56N	77E	I	338	56	283
202-1	8	62E	15N	S	98	62	15
202-2	105	77S	29W	D	195	77	151
203-1	8	25E	61N	I	98	25	241
203-2	157	68W	77N	I	247	68	283
204-1	3	24E	78N	I	93	24	258
204-2	170	67W	84N	I	260	67	276
205-1	170	56E	5N	S	80	56	5
205-2	83	86S	35W	D	173	86	145
206-1	164	53E	29S	S	74	53	331
206-2	56	67N	41W	D	326	67	221
207-1	102	37S	50E	I	192	37	230
207-2	56	63N	64E	I	326	63	296
209-1	103	31N	25W	S	13	31	25
209-2	35	77E	62S	N	125	77	118
210-1	173	22E	68S	I	83	22	292
210-2	17	70W	82S	I	287	70	262
211-1	2	44E	80S	I	92	44	280
211-2	16	47W	81S	I	286	47	261
212-1	49	44S	54E	I	139	44	234
212-2	4	56W	60N	I	274	56	300
213-1	116	70N	5W	D	26	70	185
213-2	28	85E	20S	S	118	85	340
215-1	143	58E	18N	S	53	58	18
215-2	63	75S	34W	D	153	75	146
216-1	71	73S	12W	D	161	73	168
216-2	157	79E	17N	S	67	79	17
217-1	44	42W	44S	D	314	42	224
217-2	170	62E	57S	I	80	62	303
218-1	38	57W	21S	D	308	57	201
218-2	140	73E	34S	S	50	73	326
219-1	155	70E	13S	S	65	70	347
219-2	60	78N	21W	D	330	78	201
220-1	76	20N	31E	D	346	20	149
220-2	137	80W	72S	N	227	80	72
221-1	13	44E	64S	I	103	44	296
221-2	47	51N	68W	I	317	51	248
222-1	52	44N	22W	D	322	44	202
222-2	158	75E	48S	I	68	75	312
223-1	130	38S	31W	D	220	38	149
223-2	15	72E	56N	N	105	72	56
224-1	0	56E	12S	S	90	56	348
224-2	83	80N	35W	D	353	80	215
225-1	82	27S	41E	D	172	27	221
225-2	30	73W	69N	I	300	73	291
226-1	35	31W	48S	I	305	31	228
226-2	169	67E	68S	I	79	67	292
227-1	153	65E	17S	S	63	65	343
227-2	56	75N	26W	D	326	75	206
228-1	171	41W	55N	I	261	41	305
228-2	34	57E	64N	I	124	57	244
229-1	62	75S	6W	D	152	75	174
229-2	150	84E	15N	S	60	84	15
230-1	84	62N	21W	D	354	62	201
230-2	4	72E	29S	S	94	72	331

Table 1. (*Continued.*)

Ref.	Strike	Dip	Pitch	s	*d*	*p*	*i*
231-1	142	60W	2S	S	232	60	2
231-2	53	88N	31E	D	323	88	149
232-1	178	50W	40N	S	268	50	320
232-2	60	61S	48E	I	150	61	228
233-1	153	62E	16S	S	63	62	344
233-2	55	76N	30W	D	325	76	210
234-1	65	45N	12W	D	335	45	192
234-2	164	82E	45S	S	74	82	315
235-1	144	53E	8S	S	54	53	352
235-2	49	84N	38W	D	319	84	218
236-1	7	46W	59S	I	277	46	239
236-2	146	52E	61S	I	56	52	299
237-1	87	71N	10W	D	357	71	190
237-2	0	81E	19S	S	90	81	341
238-1	119	45S	19W	D	209	45	161
238-2	15	77E	46N	N	105	77	46
239-1	99	41N	15E	D	9	41	165
239-2	178	80W	49S	N	268	80	49
241-1	115	36S	60W	N	205	36	120
241-2	151	59E	69N	N	61	59	69
242-1	166	70E	16N	S	76	70	16
242-2	82	75S	21W	D	172	75	159
243-1	83	18N	5W	D	353	18	185
243-2	178	88E	72S	I	88	88	288
245-1	48	52N	27W	D	318	52	207
245-2	155	69E	41S	S	65	69	319
248-1	73	28N	23E	D	343	28	157
248-2	142	79W	64S	N	232	79	64
251-1	7	51E	22S	S	97	51	338
251-2	83	73N	42W	D	353	73	222
252-1	13	41W	81S	I	283	41	261
252-2	1	50E	82S	I	91	50	278
253-1	34	40E	55N	I	124	40	235
253-2	172	58W	64N	I	262	58	296
254-1	14	35W	67N	I	284	35	293
254-2	41	58E	75N	I	131	58	255
255-1	22	30W	79N	I	292	30	281
255-2	35	61E	84N	I	125	61	264
258-1	24	33W	66N	I	294	33	294
258-2	52	60S	76E	I	142	60	256
259-1	14	32W	60N	I	284	32	300
259-2	48	63S	73E	I	138	63	253
260-1	28	36W	71N	I	298	36	289
260-2	51	56S	77E	I	141	56	257
262-1	3	43W	31S	D	273	43	211
262-2	117	69N	51E	I	27	69	309
264-1	71	64N	27W	D	341	64	207
264-2	174	66E	28S	S	84	66	332
265-1	66	44N	43W	D	336	44	223
265-2	10	62E	54S	I	100	62	306
266-1	68	46S	57E	I	158	46	237
266-2	25	53W	60N	I	295	53	300
269-1	74	60N	26W	D	344	60	206
269-2	178	68E	32S	S	88	68	328
271-1	35	54E	5N	S	125	54	5
271-2	128	86S	37W	D	218	86	143
273-1	120	34N	1W	S	30	34	1
273-2	31	89E	57S	N	121	89	123
274-1	146	37E	23S	S	56	37	337
274-2	37	76W	56S	I	307	76	236
276-1	35	41E	89N	I	125	41	269
276-2	34	49W	89N	I	304	49	271
277-1	170	40W	50N	I	260	40	310
277-2	38	61E	62N	I	128	61	242

Table 1. (*Continued.*)

Ref.	Strike	Dip	Pitch	s	*d*	*p*	*i*
278-1	135	46E	31S	S	45	46	329
278-2	22	68W	49S	I	292	68	229
279-1	27	38W	70S	I	297	38	250
279-2	2	55E	74S	I	92	55	286
281-1	167	34W	48N	I	257	34	312
281-2	34	65E	66N	I	124	65	246
283-1	101	19N	40E	D	11	19	140
283-2	153	78W	75S	N	243	78	75
284-1	138	53E	42S	S	48	53	318
284-2	20	58W	46S	I	290	58	226
287-1	84	9S	10E	S	174	9	10
287-2	4	88W	82N	N	274	88	98
288-1	55	20N	56W	I	325	20	236
288-2	19	74E	78S	I	109	74	282
289-1	83	32N	14E	D	353	32	166
289-2	161	83W	58S	N	251	83	58
290-1	109	21N	56E	N	19	21	124
290-2	145	73W	77S	N	235	73	77
291-1	66	54N	33W	D	336	54	213
291-2	177	64E	40S	S	87	64	320
292-1	16	55E	16N	S	106	55	16
292-2	115	77S	36W	D	205	77	144
293-1	64	37S	76E	I	154	37	256
293-2	47	54N	79E	I	317	54	281
294-1	81	37N	29W	D	351	37	209
294-2	15	73E	56S	I	105	73	304
296-1	134	28N	89W	N	44	28	89
296-2	133	62S	89W	N	223	62	91

Seismological records and GPS measurements clearly documented reverse co-seismic slip, up to about 11 m in amplitude (Ma *et al.* 1999). Earthquake source studies of the main shock showed that reverse slip occurred in a NW direction, on a fault plane dipping 25° eastward down to at least 15 km depth (Kao & Chen 2000).

This co-seismic behaviour is typical of the tectonic framework of Taiwan, which is characterized by a collision between the Philippine Sea plate and the Eurasian plate, resulting from the northern Luzon arc indenting into the Eurasian continental margin, a process that began about 5 Mya (Fig. 10a). Prior to the Chichi earthquake, the suture zone of eastern Taiwan, where NW–SE convergence occurs continuously, was considered as the plate boundary. Ironically, the good geological and geophysical knowledge revealing tectonic activity of this eastern suture zone, as well as the geodetic surveys indicating relatively little deformation in western Taiwan during the pre-Chichi period of quiescence, seemed to support this point of view. The Chichi earthquake suddenly drew attention on the importance of present-day thrust displacement across the western front of the mountain belt. The convergence rate in western Taiwan had been underestimated because it occurred through a succession of large earthquakes such as the Chichi earthquake, separated by long periods of quiescence. Simple estimates based on the amplitude of displacement during large earthquakes and the average time period of the seismic cycle in fact suggest that the convergence rates across this belt front zone and across the eastern suture zone are approximately similar in amplitude. At each of these two boundaries, the average convergence rate is about 3 cm yr^{-1}. As a result, a lithospheric model including a two-plate boundary was proposed for Taiwan (Angelier *et al.* 2001).

The large amount of high-quality data recorded by the Broadband Array in Taiwan for Seismology (BATS) allowed accurate determination of the source parameters of the Chichi earthquake sequence through waveform inversion. To process their data, Kao & Chen (2000) used an inversion algorithm adapted from Kao *et al.* (1998) and Kao & Jian (1999). They extracted the source parameters, including the centroid moment tensor and the focal depth. Furthermore, waveform inversion studies enabled Kao & Chen (2000) to distinguish five subevents in the main shock sequence. The initial subevent was relatively small and the size of the first four subevents increased as the rupture propagated from south to north (Fig. 10b). This main shock sequence was followed by numerous aftershocks invading the Taiwan island between approximate latitudes of 23°N and 24.5°N (Fig. 11). All of these focal mechanisms of the Chichi earthquake sequence were used to invert for the regional stress field associated with the Chi-Chi earthquake sequence (Kao & Angelier 2001a,b). The resulting focal mechanisms are adopted as data in this section and the next two sections, in order to illustrate the application of the new inversion method. For further regional information about earthquakes in Taiwan, the reader is referred to the papers mentioned

Table 2. Results of SSSC-based inversions: stress tensors and average misfits obtained. Data displayed in Table 1 and Fig. 11. Exp., number of experiment, as referred to in the text. The control parameter ω_{acc} indicates the smallest acceptable value of an individual estimator ω, in per cent. The stress tensor obtained is characterized by the trends and plunges of the three principal stress axes, $\boldsymbol{\sigma}_1$, $\boldsymbol{\sigma}_2$ and $\boldsymbol{\sigma}_3$, in degrees, and by Φ, the ratio of the principal stress differences defined in eq. (2). N_R, number of nodal planes rejected. N, number of nodal planes accepted. Average value of the main estimator, omega, as ω_m, in per cent. Smallest individual value found for this estimator as ω_{min}. Average value of the subsidiary estimator tau as τ_m^*, in per cent. Average value of the subsidiary estimator ang as α_m, in degrees.

Exp.	ω_{acc}	$\boldsymbol{\sigma}_1$		$\boldsymbol{\sigma}_2$		$\boldsymbol{\sigma}_3$		Φ	N_R	N	ω_m	ω_{min}	τ_m^*	α_m
1	−100	300	8	38	46	203	43	0.33	0	212	54	−57	70	34
2	0	299	8	36	41	201	48	0.29	12	200	59	1	72	30
3	10	298	6	33	41	201	48	0.31	20	192	61	12	73	29
4	20	295	5	29	38	198	52	0.32	38	174	65	23	76	25
5	30	296	5	30	37	199	53	0.29	46	166	68	32	78	24
6	40	294	4	27	36	199	54	0.27	66	146	72	43	81	22
7	50	294	5	27	33	197	57	0.27	74	138	74	51	82	21
8	60	294	5	28	38	198	51	0.31	98	114	77	60	84	19
9	70	300	10	47	57	204	31	0.48	140	72	84	71	89	15
10	80	299	10	41	51	202	37	0.51	164	48	89	81	92	13
11	90	302	16	58	56	203	28	0.53	184	28	93	91	95	9

Table 3. Individual *a posteriori* misfit values for the SSSC-based inversions. Reference numbers of data as in Table 1 and Figs 11 and 12. Columns labelled 2, 4, 6 and 8 indicate the values of the individual estimator omega (ω). These columns refer to experiments 2, 4, 6 and 8 of Table 2, with ω_{acc} chosen as 0, 20, 40 and 60, respectively. (ω_{acc}, smallest acceptable value of individual estimator ω). The last two columns indicate the two subsidiary estimators, tau and ang, for the experiment number 8: τ^*, normalized shear stress, in per cent; α_m, slip-shear angle, in degrees.

Ref.	2	4	6	8	τ^*	α
168-1	49	54	55	55*	70	39
168-2	48	54	55	55*	74	42
169-1	81	82	84	82	88	21
169-2	81	82	84	82	83	6
170-1	28	33	32*	34*	35	14
170-2	29	34	33*	35*	37	18
171-1	61	67	68	68	83	35
171-2	61	67	68	68	79	31
172-1	95	94	94	95	97	12
172-2	95	94	94	95	95	5
173-1	−63*	−64*	−64*	−64*	73	152
173-2	−62*	−64*	−63*	−64*	66	165
174-1	42	45	45	46*	86	58
174-2	42	45	45	46*	59	39
175-1	78	71	67	70	100	46
175-2	78	71	67	70	72	15
176-1	94	94	95	94	94	3
176-2	94	94	94	94	98	16
177-1	20	11*	9*	11*	35	72
177-2	20	11*	9*	11*	52	78
178-1	63	69	71	70	85	34
178-2	63	69	71	70	81	30
179-1	87	85	83	85	94	25
179-2	86	84	82	84	87	14
180-1	47	36	34*	35*	37	18
180-2	49	37	35*	36*	71	59
181-1	19	17*	22*	17*	73	77
181-2	19	16*	22*	17*	68	76
182-1	24	17*	17*	18*	44	66
182-2	23	17*	16*	17*	60	74
183-1	61	52	48	51*	99	59
183-2	60	51	47	50*	52	18
184-1	71	65	62	65	92	45
184-2	71	65	61	65	76	32
185-1	3	−9*	−14*	−10*	11	165
185-2	3	−9*	−14*	−11*	93	97
186-1	45	36	32*	35*	94	68
186-2	45	36	31*	35*	40	29
187-1	22	12*	7*	9*	68	82
187-2	23	13*	9*	11*	29	68
188-1	49	48	53	48*	83	54
188-2	48	47	53	47*	70	47
189-1	18	6*	2*	5*	19	75
189-2	18	6*	2*	5*	69	86
190-1	87	81	79	81	99	35
190-2	87	80	78	80	81	8
191-1	87	88	87	89	89	5
191-2	87	88	86	88	89	6
192-1	84	78	74	77	99	39
192-2	83	77	74	76	81	19
193-1	79	71	71	71	71	1
193-2	79	72	72	72	86	34
194-1	92	88	89	88	90	11
194-2	92	88	89	88	91	14
195-1	42	37	33*	35*	36	11
195-2	42	37	33*	35*	94	68
196-1	64	57	56	55*	60	24
196-2	64	57	57	56*	56	10
198-1	89	89	88	90	90	3
198-2	89	89	88	89	91	9
199-1	46	53	53	55*	55	7
199-2	46	53	53	54*	72	40
200-1	64	56	54	56*	98	55
200-2	64	56	54	56*	62	26
201-1	43	40	39*	38*	47	34
201-2	42	39	38*	37*	92	66
202-1	46	35	31*	33*	82	66
202-2	47	36	31*	34*	35	17
203-1	30	34	38*	35*	81	64
203-2	32	35	39*	36*	67	57
204-1	44	46	49	48*	79	53
204-2	44	47	49	48*	69	47
205-1	82	75	72	74	100	42
205-2	82	75	72	74	76	12
206-1	98	98	98	99	99	4
206-2	98	99	98	99	99	0
207-1	37	32	29*	30*	31	15
207-2	36	31	28*	29*	100	73
209-1	−4*	−4*	−7*	−3*	10	108
209-2	−5*	−5*	−8*	−4*	31	98
210-1	62	62	62	62	72	30
210-2	62	62	62	62	64	13
211-1	80	85	88	86	98	29
211-2	80	85	88	86	86	5
212-1	75	75	79	76	78	14
212-2	75	75	79	76	77	13
213-1	0*	−8*	−9*	−10*	29	111
213-2	−1*	−8*	−9*	−11*	11	169
215-1	61	59	58	60	80	41
215-2	61	59	58	60	73	34
216-1	76	72	73	73	74	10
216-2	76	72	73	73	89	35
217-1	84	89	90	89	91	10
217-2	85	89	91	90	97	23
218-1	65	73	73	74	96	40
218-2	66	73	73	74	76	11
219-1	91	91	91	92	93	10
219-2	90	91	91	92	94	12
220-1	28	29	27*	29*	33	27
220-2	28	30	27*	30*	56	58
221-1	94	95	96	95	95	1
221-2	94	95	96	94	98	16
222-1	77	81	82	82	91	26
222-2	77	81	82	82	92	27
223-1	−5*	−16*	−21*	−18*	21	149
223-2	−4*	−15*	−21*	−17*	52	109
224-1	87	81	79	80	96	33
224-2	87	81	79	80	80	5
225-1	58	51	49	50*	52	14
225-2	57	50	48	49*	68	44
226-1	67	74	75	74	75	11
226-2	68	74	76	75	95	38
227-1	90	91	92	92	93	8
227-2	90	91	92	92	94	11
228-1	58	64	70	65	68	15
228-2	59	65	71	66	69	18
229-1	71	70	73	72	72	7
229-2	70	70	72	72	83	31
230-1	77	73	73	72	73	12
230-2	77	72	73	71	72	7
231-1	37	43	48	45*	47	17

Table 3. (*Continued.*)

Ref.	2	4	6	8	τ^*	α
231-2	36	41	47	44*	77	56
232-1	65	65	71	66	76	30
232-2	64	64	70	65	69	19
233-1	90	91	91	92	93	9
233-2	90	91	91	92	93	7
234-1	73	75	76	75	83	26
234-2	73	74	75	74	86	30
235-1	74	76	75	77	80	15
235-2	73	75	74	76	77	6
236-1	56	64	65	65	81	37
236-2	56	65	66	65	82	37
237-1	74	67	68	67	72	23
237-2	74	67	68	67	67	0
238-1	13	0*	−4*	−1*	7	101
238-2	14	2*	−3*	0*	41	90
239-1	22	18*	19*	18*	21	33
239-2	22	18*	19*	17*	61	73
241-1	1	−8*	−10*	−8*	18	117
241-2	3	−7*	−9*	−7*	91	94
242-1	77	69	68	69	94	42
242-2	77	69	68	69	70	9
243-1	21	23	25*	23*	27	30
243-2	22	24	26*	24*	64	68
245-1	84	89	89	89	98	24
245-2	84	89	89	89	94	17
248-1	33	35	34*	35*	47	42
248-2	33	35	33*	35*	62	56
251-1	86	81	79	79	95	33
251-2	86	80	78	79	80	10
252-1	75	81	85	82	82	5
252-2	75	81	85	82	98	33
253-1	66	69	73	70	86	36
253-2	66	69	74	70	72	11
254-1	62	65	71	66	77	32
254-2	62	66	71	66	67	9
255-1	58	62	67	62	72	31
255-2	57	61	66	61	62	8
258-1	55	56	62	56*	78	44
258-2	54	56	61	56*	67	33
259-1	52	55	61	56*	73	41
259-2	52	54	60	55*	63	29
260-1	62	62	67	63	83	41
260-2	62	63	68	63	70	26
262-1	21	29	27*	30*	78	68
262-2	21	30	28*	30*	30	8
264-1	95	92	93	92	93	8
264-2	94	92	92	92	92	6
265-1	81	81	83	80	81	6
265-2	80	80	82	80	80	0
266-1	70	66	69	66	68	15
266-2	69	65	68	65	90	44
269-1	90	87	87	87	88	8
269-2	89	87	87	86	86	3
271-1	−7*	−14*	−19*	−17*	74	103
271-2	−7*	−14*	−19*	−16*	45	111
273-1	23	24	22*	26*	26	7
273-2	22	23	21*	24*	26	21
274-1	68	70	69	71	71	3
274-2	69	71	69	71	71	2
276-1	86	86	88	86	86	0
276-2	86	86	88	85	95	26
277-1	55	61	67	62	66	20
277-2	55	60	67	62	62	7
278-1	51	57	57	58*	60	13

Table 3. (*Continued.*)

Ref.	2	4	6	8	τ^*	α
278-2	52	57	57	58*	71	34
279-1	79	85	88	85	85	0
279-2	80	85	88	86	95	26
281-1	45	51	58	53*	59	26
281-2	45	52	58	53*	54	7
283-1	16	16*	14*	15*	20	40
283-2	16	16*	14*	15*	71	78
284-1	56	64	64	65	69	21
284-2	58	65	65	66	84	38
287-1	−22*	−16*	−14*	−16*	40	113
287-2	−22*	−16*	−15*	−16*	50	109
288-1	36	40	44	40*	46	30
288-2	35	39	43	39*	41	18
289-1	36	36	36*	36*	40	27
289-2	37	38	38*	38*	76	60
290-1	13	12*	9*	11*	20	55
290-2	14	13*	11*	13*	61	78
291-1	92	92	92	91	92	5
291-2	92	92	92	91	91	2
292-1	25	15*	9*	12*	84	82
292-2	26	15*	10*	13*	24	57
293-1	71	67	68	66	70	19
293-2	70	66	67	65	99	49
294-1	51	51	53	50*	50	7
294-2	51	51	53	50*	50	4
296-1	6	1*	−3*	0*	47	90
296-2	6	0*	−3*	0*	34	91

above in this section: Kao *et al.* (1998), Kao & Jian (1999), Ma *et al.* (1999), Kao & Chen (2000), Angelier *et al.* (2001), Kao & Angelier (2001a,b). These papers contain references to other seismotectonic studies of Taiwan.

Within a complete set of 115 focal mechanisms that belong to several seismogenic units identified by Kao & Chen (2000), nine mechanisms were removed because of their particular location in the footwall block, west of the main rupture fault. The remaining 106 mechanisms belong to the hangingwall block and the surrounding regions to the north and the south. The earthquakes of this Chichi sequence occurred from 1999 September 20th to 2000 September 16th. All foci were located in the crust, most of them at shallow depths. All local magnitudes are greater than 4; they are greater than 5 for 29 shocks and greater than 6 for 14 shocks.

The focal mechanisms are listed in Table 1 and located in Fig. 11 with the same reference index numbers. All angles have been rounded to the nearest degree. For each focal mechanism, both the nodal planes are described in Table 1, with arbitrary indices 1 and 2. Two formats are displayed for the reader's convenience (Table 1). The first format is that used to describe fault slip data in previous papers (e.g. Angelier 1990). This format includes three angles, the fault strike (0°–180°), the fault dip (0°–90°) and the pitch (0°–90°); to avoid ambiguities concerning the dip direction and the pitch orientation, a letter follows the dip angle and the pitch angle (N for north, E for east, S for south, W for east). Another letter indicates the sense of relative motion (S for left-lateral, N for normal, D for right-lateral, I for reverse). The second format is based on the three angles described in Fig. 8 and used in eqs (17) and (19), following the convention adopted by Angelier *et al.* (1982). These angles are the fault dip direction (azimuth, 0°–360°), the fault dip (0°–90°) and the pitch (0°–360°). No letter is needed, because the dip

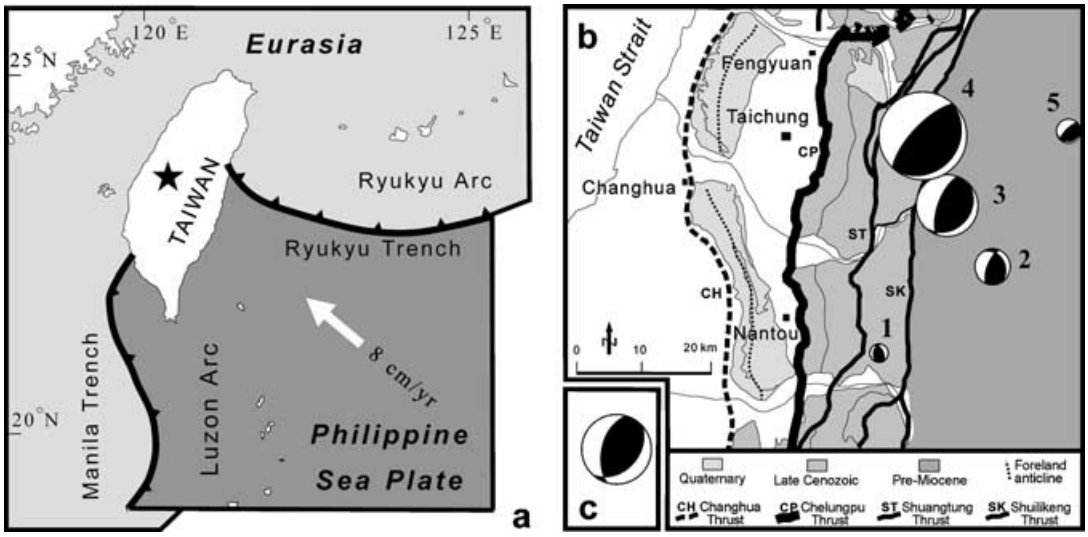

Figure 10. Plate tectonics and geological environment of the Chichi earthquake. (a) Plate tectonic framework, with the Philippine Sea Plate in dark grey and triangles on the upthrust side along subduction boundaries. An open arrow indicates the direction of plate convergence. (b) Main geological units and main shock focal mechanisms of the Chichi earthquake. Stereoplots of the focal mechanism as equal-area projections of the lower hemisphere, with tension and pressure dihedra, respectively, as black and white. Five subevents are shown on the map, as determined by Kao & Chen (2000), with numbers 1–5 indicating the order of succession, and the stereoplot size increasing with magnitude. See also Kao & Angelier (2001a) for details. Rupture trace of the 1999 Chichi earthquake is shown as a thick black line. (c) Average focal mechanism of the main shock taken as a whole.

direction is unambiguous and the pitch describes both the orientation and the sense of relative motion.

Among the 212 nodal planes of the data set (Table 1), one-half shows pitches of potential slip vectors smaller than 45°, indicating that the largest component of motion is strike-slip. For the other half of the data set, the dip-slip component of motion prevails (pitches greater than 45°); about 80 per cent of these nodal planes indicate reverse slip and the remaining ones indicate normal slip. The oblique slip geometry is common, as Figs 11 and 12 show.

The simplest experiment, referred to as 1 in Table 2, consists of a single stress tensor determination using the whole data set. No data rejection process is involved ($\omega_{\rm acc} = -100$ per cent). After this single-step inversion, a stress tensor indicating a N60°W-trending compression is obtained. The attitudes of the three principal stress axes, $\boldsymbol{\sigma}_1$, $\boldsymbol{\sigma}_2$ and $\boldsymbol{\sigma}_3$, and the ratio between principal stress differences, Φ, are given in Table 2. The average *a posteriori* omega estimator, $\omega_{\rm m}$, reaches 54 per cent, an acceptable value considering not only the uncertainties but also the dispersion and heterogeneity of the data (Fig. 12). Its smallest individual value, $\omega_{\rm min}$, is -57 per cent. The minus sign reveals inconsistency in terms of slip sense (as illustrated on the right-hand side of Fig. 9). Low positive values occur, indicating large misfits, such as for earthquake 185 (2 per cent, see Table 3, column 2). For these reasons, this first determination cannot be considered satisfactory.

It is important to take into particular consideration the largest misfits, that is, the data that cannot be accounted for by a single regional stress tensor within reasonable misfit bounds. It is necessary to examine whether these data are significant or not. This can be done through consideration of technical parameters of the individual focal mechanism determinations, magnitude and location of earthquakes, and so on. The data can be selected with objective criteria, and weighted according to a quality factor. The quality factor of the kth datum being p_k, the sum function S described in eq. (28), modified from eq. (6), thus becomes

$$S = \frac{1}{\tau_{\max}} \sum_{k=1}^{k=K} p_k \tau_{sk}. \tag{31}$$

With the focal mechanisms of Fig. 11, carrying out the inversion with non-weighted and weighted data did not result in significant differences. This showed that the variations in magnitude and technical accuracy did not influence the inversion in a significant manner. The selection of the data according to a preliminary delineation of seismogenic units resulted in more homogeneous data subsets, as discussed by Kao & Angelier (2001a,b).

Because of the methodological aim of this paper, it seemed preferable to adopt a relatively large data set, including a significant proportion of inconsistent data and non-negligible sources of dispersion. This choice enables one to better discuss and highlight the robustness of the method. The inconsistent data mainly result from dispersion and atypical mechanisms, and hence were withdrawn through a refining process. Many data sets are more homogeneous and can be analysed on a single-step basis, with none of the data being thrown out. Using the refining process is not compulsory. However, one should keep in mind that in the single-step inversion the result can be vitiated if too many data conflict with the mechanically homogeneous subset.

13 APPLICATION OF DATA SELECTION PROCESS

As mentioned in Section 11, the inversion can be included in an iterative process that aims to separate the data set into mechanically homogeneous subsets, or at refining this set through the elimination of the most inconsistent data. The latter technique is adopted hereafter. Rejecting data modifies the data set, and hence requires a new inversion to re-determine the stress. Because the new stress tensor differs from the previous one, a rejected datum may become

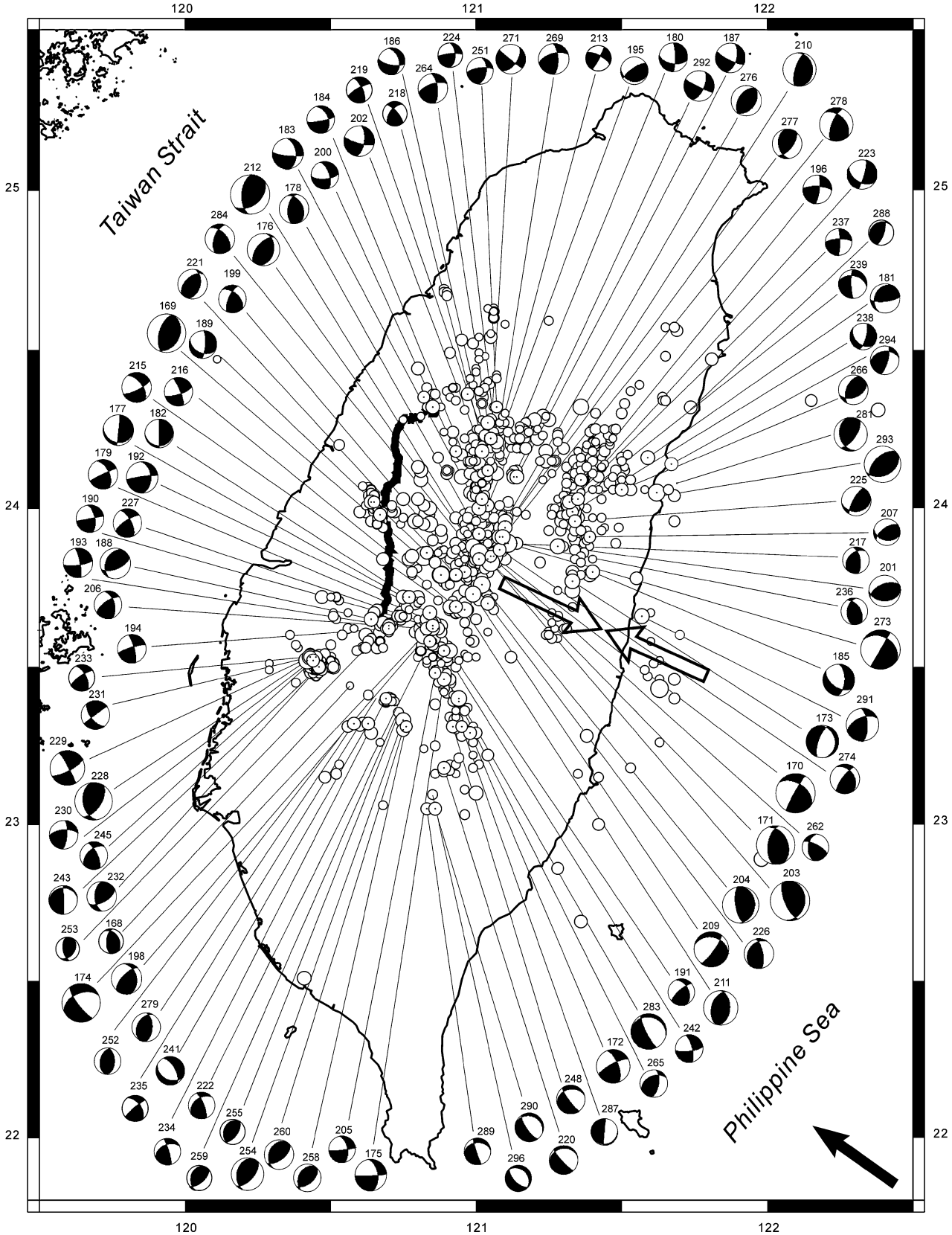

Figure 11. Data set analysed in this paper. Focal mechanisms of 106 earthquakes of the Chichi sequence determined by Kao & Chen (2000). Double couple mechanisms shown as stereoplots (equal area projection of the lower hemisphere) of tension and pressure dihedra (black and white, respectively). Same reference numbers as in Table 1. The size of the stereoplots and open dots (indicating epicentres) increases with magnitude (in the range 4–7 for earthquakes with focal mechanisms). The rupture trace of the 1999 Chichi earthquake is shown as a thick black line. A double open arrow indicates the direction of compression as indicated by the SSSC-based inversion (see Table 2 for details). The simple black arrow indicates the direction of plate convergence.

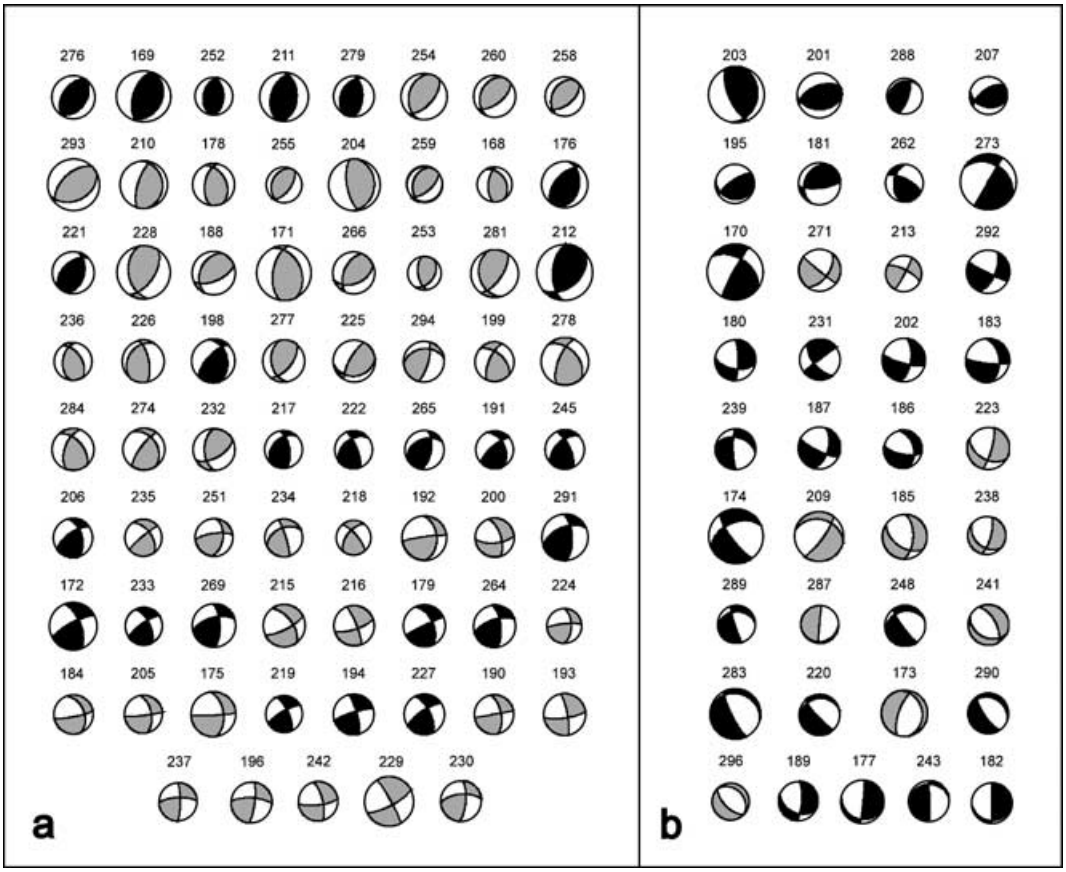

Figure 12. Classification of data based on individual *a posteriori* misfits. Same data as in Fig. 11 and Table 1. Stress tensor results are given in Table 2 (experiment 7). (a), retained focal mechanisms with ω estimators larger than 80 per cent (black and white stereoplots) or from 50 to 80 per cent (grey and white stereoplots). (b), rejected focal mechanisms with ω estimators negative (grey and white stereoplots) or from zero to 50 per cent (black and white stereoplots). Details are given in the text.

acceptable in the next step, and a retained datum may become incompatible with the new solution. Consequently, the refining process requires caution and must be carried out in a gradual way.

The minimum fit, ω_{acc}, started from −100 per cent and increased linearly. Each step involved two stress inversions. The data were progressively selected until none of the retained data displayed an individual estimator ω larger than ω_{acc}. A rejected datum could be reincorporated in a later step of the process. To control the variation of the minimum acceptable individual fit, a very small increment could be adopted because the single-step runtime is negligible. In the case of experiments 2–11 of Table 2, this increment was 0.1 per cent, so that about 3000 stress inversions were performed at stage 11. Larger increments reduced the number of stress tensors to a few tens or hundreds, and did not modify the final result.

The first experiment involving data rejection, called 2 in Table 2, aimed at finding the best-fitting data set without any inconsistent sense of slip. Accordingly, ω_{acc} was set to zero. Eight nodal planes from four focal mechanisms were eliminated. Note that for each experiment asterisks following the individual omega values have been added in Table 3 to pinpoint the rejected data. Not surprisingly, this refining process resulted in a better *a posteriori* average main estimator, ω_m, than the inversion of the total data set (59 per cent instead of 54 per cent, see Table 2). The stress tensor of experiment 2 does not differ markedly from that of experiment 1 (done without data rejection): the changes in both the principal axis attitudes and the stress difference ratio are minor (Table 2).

The values of the average subsidiary estimators, τ_m^*, and α_m, 72 per cent and 30°, respectively, for experiment 2, deserve consideration. Whereas the first one is acceptable, the average shear-slip angle is too large to be considered satisfactory in light of the angular accuracy of the focal mechanisms of earthquakes. Experiments 2–11 of Table 2 have been extracted for ten equally spaced values of ω_{acc}, from 0 to 90 per cent. Because of the increasing severity in the fitting demand, the number of rejected data increased from 12 to 184. Accordingly, the average main estimator, ω_m, increased from 59 to 93 per cent. The average subsidiary estimators increased from 72 to 95 per cent (τ_m^*) and decreased from 30° to 9° (α_m). The last value of α_m, 9°, is smaller than the average angular uncertainty of the focal mechanisms. This denotes exaggerated severity for high values of ω_{acc}. It is thus necessary to define within the gradual refining process the experiment, and hence the value of ω_{acc}, that best fits the actual constraints of the data set.

Considering the uncertainties, the data dispersion and the mechanical heterogeneity, a 60 per cent level for ω_{acc} represents a good minimum fit; 114 of the 212 data were thus retained (experiment 8, Table 2). The resulting average estimators, ω_m, τ_m^* and α_m, were 77, 84 per cent and 19°, reasonable values in light of data uncertainties and dispersion. These estimators can even be regarded as very good, taking into additional account the fan-shaped pattern of stress trajectories, which resulted in further dispersion inside the broad area where the aftershocks occurred. This particular source of regional stress variation, which was documented by a seismotectonic

analysis of the Chichi earthquake sequence, is beyond the scope of the present paper (Kao & Angelier 2001b). This suggests that even the experiments with ω_{acc} levels lower than 60 per cent provide reliable results in terms of the regional stress pattern (Table 2).

This inference is supported by the similarity of the stress tensor results listed in Table 2. Even when the demand for a good fit becomes exaggeratedly loose (experiments 2–4) or severe (experiments 9, 10 and 11), the solution does not vary markedly. The variation in the calculated trend of compression (N58°W to N66°W) is only 8° for all the experiments of Table 2. That similar tensors are obtained for a wide range of ω_{acc} values (−100 per cent to +90 per cent) shows that the solution is stable. Had the data set contained two or more subsets corresponding to independent states of stress, this would not have been the case. There is a reliable, albeit non-unique, relationship between the stability of the solution and the mechanical homogeneity of the data set. Thus, in addition to the basic single-step inversion (Table 2, row 1), the refining process (Table 2, rows 2–11) enables one to evaluate the robustness of the stress tensor determination.

14 INDIVIDUAL RESULTS OF THE INVERSION

In the previous section, the conclusions were mainly based on consideration of the average estimators, although the refining process was by definition controlled by an individual parameter, the smallest acceptable fit level (ω_{acc}). The individual estimators enable one to evaluate how far the stress tensor solution accounts for each focal mechanism of the earthquake. The *a posteriori* values of ω are listed in Table 3 for experiments 2, 4, 6 and 8 (respectively, corresponding to 0, 20, 40 and 60 per cent for ω_{acc}), and for experiment 8 the values of τ^* and α have been added.

The differences in the two individual estimators ω of a focal mechanism remained small (Table 3); these minor discrepancies mainly arose because the three angles describing each nodal plane had been rounded to the nearest integer value in degrees, slightly altering the perpendicular relationships of Fig. 4. Compared with the uncertainties, this difference is negligible so that the two numerical values of ω obtained for each mechanism should be regarded as identical. In contrast, different values of τ^* and α may be obtained, highlighting the properties of double couple mechanisms of earthquakes illustrated in Figs 3 and 6.

Different individual behaviours emerge from the comparison between successive experiments, in terms of the main estimator, ω (this would be *a fortiori* the case for the subsidiary estimators). On one hand, many mechanisms displayed similar misfits during the succession of experiments, whatever the value of ω_{acc} (from 0 to 60 per cent, see Table 3). This was the case for the permanently well-fitting mechanisms like 172 (ω remaining above 90 per cent), or the permanently inconsistent ones like 173 (ω remaining below −60 per cent). This was also the case for many mechanisms displaying nearly constant intermediate fitting levels throughout the sequence of experiments, like 168 (48–55 per cent) or 181 (16–22 per cent). On the other hand, many mechanisms showed significant variations in fitting levels. As ω_{acc} increases, the mechanism may display fit degradation, like 189 (from 18 to 5 per cent) or improvement, like 236 (from 56 to 65 per cent). The minor changes (2 per cent or less) being left aside, the variation of ω may be monotonic (most cases) or not (like 175, with degradation followed by improvement, or 188, the opposite case).

The individual values of normalized shear stress (τ^*) and slip-shear angle (α) given in Table 3 for experiment 8 reveal high levels of variability. Not only do these estimators vary widely depending on the focal mechanism considered, but also large contrasts may exist between the two nodal planes of a given mechanism, like 174 for τ^* (86 and 59 per cent) or 183 for α (59° and 18°). In these cases, these contrasts are not independent. For mechanism 175, the nodal plane 1 better fits the stress than 2 in terms of normalized shear stress (100 per cent versus 72 per cent), but not in terms of slip-shear angle (46° versus 15°). This is not surprising considering that for a given SSSC value an increase in α requires an increase in τ^* (Fig. 9). The two nodal planes may show identical or similar values for both τ^* and α: this is the case for well-fitting mechanisms like 191 (89 per cent and 5°–6°, respectively) and inconsistent ones like 287 (40–50 per cent and 113–109°, respectively).

It is important to observe that the *a posteriori* choices between nodal planes, based on consideration of the normalized shear stress on one hand and the slip-shear angle on the other hand, lead to different conclusions. Some mechanisms, like 274, show excellent slip-shear angles (2°–3°) but relatively low shear stress (71 per cent); other ones, like 236, reveal high normalized shear stress (81–82 per cent) but poor slip-shear angles (37°). This contrast brings confirmation that the SSSC dual-criterion represents a compromise between the two aims as mentioned in Section 4, that is, obtaining the smallest possible slip-shear angles and reaching a relatively high level of shear stress at the same time. To go further with the investigation of the slip-shear relationships, and hence decide which subcriterion must be given priority, it would be necessary to consider friction.

Finally, it is appropriate to examine the geometry of the focal mechanisms as a function of the misfit levels indicated by the inversions. The data set is subdivided into two main subsets according to the *a posteriori* value of the estimator ω (Fig. 12). The first subset is composed of the 69 focal mechanisms (138 nodal planes) that fit the stress tensor for the 50 per cent ω level. Most of these mechanisms are reverse and strike-slip in type (top and bottom row groups of Fig. 12a, respectively). Oblique slip is common, showing in almost all cases a reverse component of slip (central rows of Fig. 12a). This reverse component is easily detectable as the centre of the stereoplot falls in a non-blank, tension domain. Few mechanisms, like 200, however, display a normal component. For strike-slip mechanisms, both the right- and left-lateral nodal planes shows large variations in strike (e.g. mechanisms 219 and 194). Among the pure reverse mechanisms, large differences in the trends of nodal planes occur (e.g. mechanisms 293 and 204). The variations in pitch for the strike-slip mechanisms and in strike for the reverse ones account for the largest component of the individual estimator dispersion. In more detail, two fitting levels have been distinguished, with estimators ω higher than 80 per cent (black and white stereoplots in Fig. 12a) and from 50 to 80 per cent (grey and white stereoplots). The latter class displays larger variation in terms of strikes and dips of nodal planes, and pitches of inferred slip vectors.

The second subset is composed of 37 mechanisms (74 nodal planes) that could not fit the minimum requirement for the 50 per cent ω level. Within this subset, 27 mechanisms revealed positive estimators ω (ranging from 0 to 50 per cent, black and white stereoplots in Fig. 12b), indicating compatibility with the stress tensor restricted to the slip sense. The 10 remaining mechanisms (negative values of ω, grey and white stereoplots) are incompatible even in terms of slip sense.

From the geometrical point of view, many mechanisms in the non-fitting subset of Fig. 12(b) resemble those of the first subset; they simply show larger angular dispersion. The reverse-type mechanisms display a large variation in trends; some couples of nodal planes even strike at nearly right angles, like 203 and 201. The

oblique-slip mechanisms display a large variety of strike, dip and pitch angles. Some strike-slip sense-consistent mechanisms, like 170 and 292, reveal a nearly opposite distribution of pressure and tension dihedra, which reveals a variation of almost 90° in the strikes of the nodal planes. The sense-inconsistent character of the strike slip-mechanisms shown in grey in Fig. 12(b), like 271, is clearly expressed because their tension dihedra contain the trend in compression indicated by the inversion (see Table 2).

Other types of mechanisms appear in the non-fitting subset, whereas they were not found in the first subset. The presence of mechanisms with a nearly vertical dip-slip nodal plane and a nearly horizontal strike-slip one becomes common (e.g. the last three mechanisms, 177, 243 and 182, in Fig. 12b). Such a configuration was absent in the well-fitting subset, although some mechanisms were close to it (e.g. mechanisms 225 and 274 in Fig. 12a). The normal type, absent in the best-fitting subset of Fig. 12(a), is present in the subset of Fig. 12(b), even among the sense-consistent mechanisms like 290 (the intersection of nodal planes striking nearly parallel to the trend of compression). Among the sense-inconsistent mechanisms, normal-type mechanisms are also common, with a larger trend in dispersion (compare mechanisms 173 and 296 in Fig. 12b).

Choosing the boundary between the fitting and non-fitting subsets, as in Fig. 12(a), is subject to debate, because no significant gap occurs in the range of ω values. A rigorous choice can be made as a function of both the technical uncertainties in focal mechanism determinations and the natural sources of dispersion that are more difficult to evaluate. Large stress variations are known to occur in the crust. For instance, a significant clockwise change in the trend of the compression from south to north has been reconstructed in the area of Fig. 11 (Kao & Angelier 2001a,b). This change, not to mention other variations in stress axes and ratio Φ, results in a dispersion that is larger than the technical uncertainty.

The large dispersion is not surprising if one considers the perturbations of the regional stress field. This is especially important after a large earthquake such as the Chichi earthquake, because all the dislocations associated with the highly heterogeneous faulting of the whole aftershock sequence result in a major perturbation of the regional stress field. It is well known, for instance, that the perturbation field can be larger than the original stress field, especially near the dislocation edges; the aftershock sequence may also be deeply influenced by the weakness structure in and around the main fault plane. For this reason, it is interesting to note that even in a highly perturbed stress environment it was possible to reconstruct a regional average stress state accounting for most of the data, as shown by the experiments listed in Table 2. That the estimators remain within acceptable bounds, given the accuracy and dispersion of the data, suffices to demonstrate that the stress tensor obtained with the drastic assumption of homogeneous stress is significant regionally. Note that the inversion is carried out in terms of axis orientations and Φ ratio, so that absolute stress magnitudes are left free in terms of the two remaining unknowns, k and l (see Section 7). Furthermore, the stress tensor obtained accounts for the mechanisms of the main shock (see Kao & Angelier 2001b, for details).

These observations, albeit empirical, bring confirmation that regardless of the technique adopted the inversion of focal mechanisms to reconstruct an average stress tensor has the capacity to overcome the difficulties related to stress perturbations and crustal heterogeneity. It should be borne in mind, however, that because of the dispersion it is preferable to carry out the inversion in one of the following ways. With big data sets covering a large area, the large number of data points compensates the dispersion and the average stress tensor obtained has a regional value; its significance can be evaluated through a review of the misfit distribution. With data sets in a narrow window (such sets often being small), the dispersion commonly decreases and the stress tensor obtained has a local value, with rather tightly clustered misfits (see examples for the Chichi sequence in Kao & Angelier 2001a,b). Drawing conclusions from the inversion of small data sets covering large crustal volumes requires more caution, because the stress perturbations discussed above may drastically influence the result and can hardly be detected by considering the distribution of the misfits, which is not statistically significant with low numbers of data points.

In the case presented in this paper, the N–S variation in the trend of the compression, as well as the other sources of dispersion, remained of second order compared with the major seismotectonic regime, a WNW–ESE-trending compression related to plate collision (Fig. 11). The separation into subsets based on the location of earthquake epicentres or the delineation of seismogenic units allowed determination of stress subregimes in the second approximation (Kao & Angelier 2001a), but did not invalidate the determination of a major regional stress regime made in the first approximation. In these respects, the choice of the discriminating value, such as 50 per cent for ω in Fig. 12, is related to the scale and approximation levels of the analysis and cannot be uniquely defined. More important is the stability of the stress tensor determined with different levels of acceptable misfit: the comparative analysis revealed high stability (Table 2), which supports the determination of a single stress tensor in the first approximation.

15 COMPARISON WITH OTHER METHODS

To compare the results with those obtained from other inversion methods, a difficulty arises because the new technique does not require the choice between the nodal planes, whereas the previous ones did. However, it is possible to choose the results of the *a posteriori* separation discussed in the previous section, and thus to compare stress inversions carried out with identical data sets of N nodal planes (that is, one nodal plane selected for each focal mechanism). This has been done using the inversion method described previously in this journal (Angelier 1990). The results are almost identical in terms of the resulting stress tensors. The difference cannot be regarded as significant, and results from two main factors. First, the inversion criteria differ: the function maximized with the new technique is the SSSC, or shear stress slip component, τ_s (Fig. 1), whereas in the previous direct inversion method the function minimized was the magnitude of the vector difference $\mathbf{s}-\boldsymbol{\tau}$ (Angelier 1990). Secondly, as discussed in Section 5, the best results with the new technique were obtained when using the sum defined in eq. (28), adapted from eq. (6), which does not fulfil the least-squares criterion. In contrast, a typical least-squares minimization was involved in the direct inversion method. This difference implies that the influence of each datum is not the same in both analyses, depending on the misfit amplitude.

The results obtained with the new technique were also compared with those issued from the P and T dihedra method, or 'right dihedra method' (Angelier & Mechler 1977). This comparison could not go very far, because the right dihedra method is based on consideration of the mechanical compatibility between the double couple focal mechanisms and does not involve determination of a stress tensor and related estimators. Furthermore, with the right dihedra approach the requirements for mechanical compatibility between

all focal mechanisms are not fully exploited, so that the results are confidence domains, not optimal orientations (see the explanation in Angelier & Mechler 1977). On the other hand, a major point of interest in the right dihedra method, in addition to its geometrical simplicity, is the absence of any choice between nodal planes, so that the comparison with the new method is straightforward. Not surprisingly, the principal stress axes obtained in this paper fall within the confidence domains obtained with this earlier method.

16 NUMBER OF DATA REQUIRED IN THE INVERSION

A crucial aspect in the inversion of fault slip data or earthquake focal mechanisms is the number of data required in the inversion. In theory, four independent focal mechanisms are sufficient to determine the four unknowns of a reduced stress tensor, as discussed in Section 7. In practice, large data sets are required to reliably determine the regional stress, because of the data uncertainties and dispersion. It is impossible, however, to give rigid bounds to the number of data required in the inversion, because it depends strongly on these two factors. Little difficulty comes from the angular uncertainties in focal mechanisms, because they are easily estimated based on technical considerations (the number and distribution of the stations used, nature of wave data, misfits, etc.). Determining the dispersion factor is more complex, because it results from the difference between the assumption of a unique reduced stress tensor accounting for the data, and the real situation that may involve complex stress variations in time and space within the studied data set. Consequently, the dispersion factor increases with the rock volume considered, because the larger the volume the higher the sources of stress variation. However, the amount of dispersion may differ significantly depending on the regional structural geology. In the case of the fold and thrust belt of Taiwan (a highly deformed and inhomogeneous structure), this dispersion is much larger than the technical uncertainties of focal mechanism determinations. This dispersion explains why a high percentage of the data must be discarded to reach good fitting levels in such a complex crustal domain. When one studies smaller geological units, the dispersion diminishes and the process commonly ends up discarding a small percentage of data. In contrast to technical uncertainties, the dispersion factor is difficult to quantify prior to the inversion; its best determination certainly comes from the *a posteriori* reviews.

It is concluded that the number of data required to obtain reliable stress inversion is variable, as a function of these two factors. As discussed in Sections 13 and 14, the uncertainties in the determination of the focal mechanisms of Fig. 11 were limited because of the earthquake magnitudes and the quality of the seismological network. However, the dispersion was large because of the size and structural complexity of the area studied. The angular uncertainty of the focal mechanism determinations averaged 10 (Kao & Chen 2000), and the angular dispersion of the data set, which depends on the heterogeneous response of the volume of crust affected by these earthquakes, cannot be less than 12°. This leads one to favour, for this data set, the solution obtained for a 40 per cent value of ω_{acc}, because it gives 22° for α_m (Table 2). A separation into subsets defined according to the preliminary delineation of seismically homogeneous domains has been presented elsewhere (Kao & Angelier 2001a); it provided reliable determinations with a small number of data points (e.g. 10). Large sets are, however, preferable, because of their potential to allow determination of internal levels of mechanical consistency on an acceptable statistical basis.

17 CONCLUSION

The new method presented in this paper enables one to determine the stress state that best accounts for a set of double couple focal mechanisms of earthquakes. No choice between the nodal planes is needed prior to, or made during, the inversion. This method is based on consideration of the SSSC criterion. Because the inversion is carried out by analytical means, the runtime is negligible regardless of the size of the data set. This permits inclusion of the inversion in a variety of processes for separating or refining the data. It is difficult to evaluate the real data dispersion, which depends on complex geological factors and is as important as, or larger than, the angular uncertainties in the determination focal mechanisms. It is pointed out herein that the most efficient way to determine whether the stress inversion is significant or not consists of comparing series of refining experiments conducted with increasing demands for good fits. When they can be obtained, the stability of the stress tensor determinations throughout such successive experiments and the consistency in the distribution of individual misfits provide a good indication of a robust solution.

ACKNOWLEDGMENTS

The Institut Universitaire de France supported this research. The data taken as an example were provided by Dr Honn Kao, Academia Sinica, Taipei. Dr François Cornet, IPGP, Paris, drew the author's attention on the comparison with Tresca's criterion. Useful comments from Paul Davis and an anonymous referee resulted in a significant improvement in the paper.

REFERENCES

Anderson, E.M., 1942. *The Dynamics of Faulting,* 2nd edn, Oliver & Boyd, Edinburgh, p. 206.

Angelier, J., 1975. Sur l'analyse de mesures recueillies dans des sites faillés: l'utilité d'une confrontation entre les méthodes dynamiques et cinématiques, *C.R. Acad. Sci. Paris,* D, **281,** 1805–1808. (Erratum: 1976. *C.R. Acad. Sci. Paris,* D, **283,** 466.)

Angelier, J., 1984. Tectonic analysis of fault slip data sets, *J. geophys. Res.,* **89,** 5835–5848.

Angelier, J., 1989. From orientation to magnitudes in paleostress determinations using fault slip data, *J. struct. Geol.,* **11,** 1/2,37–50.

Angelier, J., 1990. Inversion of field data in fault tectonics to obtain the regional stress—III: a new rapid direct inversion method by analytical means, *Geophys. J. Int.,* **103,** 363–376.

Angelier, J., 1991. Inversion directe et recherche 4-D: comparaison physique et mathématique de deux modes de détermination des tenseurs de paléocontraintes en tectonique de failles, *C.R. Acad. Sci. Paris,* II, **312,** 1213–1218.

Angelier, J., 1998. A new direct inversion of earthquake focal mechanisms to reconstruct the stress tensor, *Proc. EGS XXIII Gen. Assembly, Annales Geophysicae,* **16,** suppl. 1, C115.

Angelier, J. & Mechler, P., 1977. Sur une méthode graphique de recherche des contraintes principales également utilisable en tectonique et en séismologie: la méthode des dièdres droits, *Bull. Soc. géol. France,* **7,** XIX, 6, 1309–1318.

Angelier, J., Tarantola, A., Manoussis, S. & Valette, B., 1982. Inversion of field data in fault tectonics to obtain the regional stress. 1: single phase fault populations: a new method of computing the stress tensor, *Geophys. J. R. astr. Soc.,* **69,** 607–621.

Angelier, J. *et al.*, 2001. Le séisme de Chichi et sa place dans l'orogène de Taiwan: results from source parameters and stress tensor inversions, *C.R. Acad. Sci. Paris,*II, **333,** 5–21.

Bott, M.H.P., 1959. The mechanisms of oblique slip faulting, *Geol. Mag.,* **96,** 109–117.

Carey, E. & Brunier, B., 1974. Analyse théorique et numérique d'un modèle mécanique élémentaire appliqué à l'étude d'une population de failles, *C.R. Acad. Sci. Paris,* D, **279,** 891–894.

Dupin, J.-M., Sassi, W. & Angelier, J., 1993. Homogeneous stress hypothesis and actual fault slip: a distinct element analysis, *J. struct. Geol.,* **15,** 8, 1033–1043.

Etchecopar, A., Vasseur, G. & Daignières, M., 1981. An inverse problem in microtectonics for the determination of stress tensors from fault striation analysis, *J. struct. Geol.,* **3,** 51–65.

Gephart, J.W., & Fortsyth, D.W., 1984. An improved method for determining the regional stress tensor using earthquake focal mechanism data: an application to the San Fernando earthquake sequence, *J. geophys. Res.,* B, **89,** 9305–9320.

Kao, H. & Angelier, J., 2001a. The Chichi earthquake sequence, Taiwan: results from source parameters and stress tensor inversions, *C.R. Acad. Sci. Paris,* II, **333,** 65–80.

Kao, H. & Angelier, J., 2001b. Stress tensor inversion for the Chi-Chi earthquake sequence and its implications on regional collision, *Bull. seism. Soc. Am.,* **91,** 5,1028–1040.

Kao, H. & Chen, W.-P., 2000. The Chi-Chi earthquake sequence: Active, out-of-sequence thrust faulting in Taiwan, *Science,* **30,** 2346–2349.

Kao, H. & Jian, P.-R., 1999. Source parameters of regional earthquakes in Taiwan: July 1995–December 1996, *Terr. Atmos. Oceanic Sci.,* **10,** 585–604.

Kao, H., Jian, P.-R., Ma, K.-F., Huang, B.-S. & Liu, C.-C., 1998. Moment-tensor inversion for offshore earthquakes east of Taiwan and their implications to regional collision, *Geophys. Res. Lett.,* **25,** 3619–3622.

Ma, K.-F., Lee, C.-T., Tsai, Y.-B., Shin, T.-C. & Mori, J., 1999. The Chi-Chi, Taiwan earthquake: large surface displacements on an inland thrust fault, *EOS, Trans. Am. geophys. Un.,* **80,** 605–611.

Mercier, J.-L. & Carey-Gailhardis, S.E., 1989. Regional state of stress and characteristic fault kinematics instabilities shown by aftershock sequence: the aftershock sequences of the 1978 Thessaloniki (Greece) and 1980 Campania-Lucania (Italy) earthquakes as examples, *Earth planet. Sci. Lett.,* **92,** 247–264.

Michael, A., 1984. Determination of stress from slip data: fault and folds., *J. geophys. Res.,* B, **89,** 11 517–11 526.

Reches, Z., 1987. Determination of the tectonic stress tensor from slip along faults that obey the Coulomb yield criterion, *Tectonics,* **6,** 849–861.

Wallace, R.E., 1951. Geometry of shearing stress and relation to faulting, *J. Geol.,* **59,** 118–130.